

# International Evaluation Co-operation

## Volume 34

Co-ordinated Evaluation  
of Plutonium-239 in the  
Resonance Region



## Co-ordinated Evaluation of Plutonium-239 in the Resonance Region

*A report by the Working Party  
on International Nuclear Data Evaluation Co-operation  
of the NEA Nuclear Science Committee*

***Co-ordinator***

*C. De Saint Jean*  
Nuclear Energy Division, CEA  
France

***Monitor***

*R.D. McKnight*  
Argonne National Laboratory  
United States

© OECD 2014

NUCLEAR ENERGY AGENCY

ORGANISATION FOR ECONOMIC CO-OPERATION AND DEVELOPMENT

## ORGANISATION FOR ECONOMIC CO-OPERATION AND DEVELOPMENT

The OECD is a unique forum where the governments of 34 democracies work together to address the economic, social and environmental challenges of globalisation. The OECD is also at the forefront of efforts to understand and to help governments respond to new developments and concerns, such as corporate governance, the information economy and the challenges of an ageing population. The Organisation provides a setting where governments can compare policy experiences, seek answers to common problems, identify good practice and work to co-ordinate domestic and international policies.

The OECD member countries are: Australia, Austria, Belgium, Canada, Chile, the Czech Republic, Denmark, Estonia, Finland, France, Germany, Greece, Hungary, Iceland, Ireland, Israel, Italy, Japan, Luxembourg, Mexico, the Netherlands, New Zealand, Norway, Poland, Portugal, the Republic of Korea, the Slovak Republic, Slovenia, Spain, Sweden, Switzerland, Turkey, the United Kingdom and the United States. The European Commission takes part in the work of the OECD. OECD Publishing disseminates widely the results of the Organisation's statistics gathering and research on economic, social and environmental issues, as well as the conventions, guidelines and standards agreed by its members.

*This work is published on the responsibility of the OECD Secretary-General.  
The opinions expressed and arguments employed herein do not necessarily reflect the official  
views of the Organisation or of the governments of its member countries.*

### NUCLEAR ENERGY AGENCY

The OECD Nuclear Energy Agency (NEA) was established on 1 February 1958. Current NEA membership consists of 31 OECD member countries: Australia, Austria, Belgium, Canada, the Czech Republic, Denmark, Finland, France, Germany, Greece, Hungary, Iceland, Ireland, Italy, Japan, Luxembourg, Mexico, the Netherlands, Norway, Poland, Portugal, the Republic of Korea, the Russian Federation, the Slovak Republic, Slovenia, Spain, Sweden, Switzerland, Turkey, the United Kingdom and the United States. The European Commission also takes part in the work of the Agency.

The mission of the NEA is:

- to assist its member countries in maintaining and further developing, through international co-operation, the scientific, technological and legal bases required for a safe, environmentally friendly and economical use of nuclear energy for peaceful purposes, as well as
- to provide authoritative assessments and to forge common understandings on key issues, as input to government decisions on nuclear energy policy and to broader OECD policy analyses in areas such as energy and sustainable development.

Specific areas of competence of the NEA include the safety and regulation of nuclear activities, radioactive waste management, radiological protection, nuclear science, economic and technical analyses of the nuclear fuel cycle, nuclear law and liability, and public information.

The NEA Data Bank provides nuclear data and computer program services for participating countries. In these and related tasks, the NEA works in close collaboration with the International Atomic Energy Agency in Vienna, with which it has a Co-operation Agreement, as well as with other international organisations in the nuclear field.

This document and any map included herein are without prejudice to the status of or sovereignty over any territory, to the delimitation of international frontiers and boundaries and to the name of any territory, city or area.

Corrigenda to OECD publications may be found online at:

### © OECD 2014

You can copy, download or print OECD content for your own use, and you can include excerpts from OECD publications, databases and multimedia products in your own documents, presentations, blogs, websites and teaching materials, provided that suitable acknowledgment of the OECD as source and copyright owner is given. All requests for public or commercial use and translation rights should be submitted to [rights@oecd.org](mailto:rights@oecd.org). Requests for permission to photocopy portions of this material for public or commercial use shall be addressed directly to the Copyright Clearance Center (CCC) at [info@copyright.com](mailto:info@copyright.com) or the Centre français d'exploitation du droit de copie (CFC) [contact@cfcopies.com](mailto:contact@cfcopies.com).

## Foreword

The Working Party on International Nuclear Data Evaluation Co-operation (WPEC) has been established under the aegis of the OECD/NEA Nuclear Science Committee (NSC) to promote the exchange of information on nuclear data evaluations, validation and related topics. Its aim is also to provide a framework for co-operative activities between the members of the major nuclear data evaluation projects. This includes the possible exchange of scientists in order to encourage co-operation. Requirements for experimental data resulting from this activity are compiled. The WPEC determines common criteria for evaluated nuclear data files with a view to assessing and improving the quality and completeness of evaluated data.

The parties to the project are: BROND (Russian Federation), ENDF (United States), JENDL (Japan) and JEFF (other NEA Data Bank member countries), as well as CENDL (China) in close co-operation with the Nuclear Data Section of the International Atomic Energy Agency (IAEA).

This report has been issued by the WPEC Subgroup 34 with a view to solving a general discrepancy when calculating criticality benchmarks with plutonium, using the most recent evaluated data libraries. This international effort enabled the delivery of a single set of resonance parameters up to 2.5 keV. The large fluctuations of the prompt neutron multiplicities were correctly reproduced with a phenomenological decomposition of the multiplicity that involved the two-step (n, $\gamma$ f) process. Performances of the new  $^{239}\text{Pu}$  evaluation were tested over a broad set of integral data (ICSBEP, mock-up experiments performed in the CEA facilities and in power reactors). An overall good agreement was achieved between the calculations and the experimental results.

The opinions expressed in this report are those of the authors only and do not necessarily represent the position of any member country or international organisation.

## **Members of Subgroup 34**

### **CEA Cadarache (France)**

Cyrille De Saint Jean

Gilles Noguère

Yannick Peneliau

David Bernard

Olivier Serot

### **Oak Ridge National Laboratory (USA)**

Luiz Carlos Leal

Herve Derrien

### **Los Alamos National Laboratory (USA)**

Albert C. Kahler

### **Argonne National Laboratory (USA)**

Richard D. McKnight

## Acknowledgements

Dick McKnight, the monitor and one of the main initiators of this Subgroup, passed away on August 28, 2013. With deep regret, all the members of the Subgroup want to dedicate the present report to his memory: his contribution in this project has been essential, like in many other NEA activities. During more than three decades, his outstanding knowledge, scientific vision and technical suggestions have played a key role in defining the right issues and the most appropriate approaches to solve them. Dick had extraordinary human qualities and has been a true friend to most of us. He will be greatly missed.

## Table of contents

<b>1. Introduction .....</b>	<b>8</b>
<b>2. Tasks .....</b>	<b>9</b>
<b>3. Illustrative ICSBEP benchmark: Description and initial results .....</b>	<b>11</b>
3.1 Initial result with ENDF library .....	11
3.2 Initial result with JEFF libraries (from JEFF-3.1 to JEFF-3.1.1) .....	12
3.3 Selected ICSBEP Pu-SOL-THERM set .....	12
<b>4. Re-evaluation of the <sup>239</sup>Pu resolved resonance parameters in the energy range 10<sup>-5</sup> eV to 2.5 keV .....</b>	<b>14</b>
4.1 Introduction .....	14
4.2 General descriptions .....	14
4.3 ORNL/CEA New <sup>239</sup> Pu Evaluation in the energy range 10 <sup>-5</sup> eV to 2.5 keV .....	15
4.4 Resonance Parameter Covariance Matrix (RPCM) .....	19
<b>5. Prompt neutron multiplicity in the resonance range .....</b>	<b>29</b>
5.1 Investigation of the two-step (n,γf) process .....	29
5.2 Study of the channel spin dependence of v <sub>p</sub> (E) .....	30
<b>6. Integral validation of the <sup>239</sup>Pu resolved resonance range .....</b>	<b>34</b>
6.1 Integral validation based on JEFF-3.1.1 + SG34 <sup>239</sup> Pu .....	34
6.2 Integral validation based on ENDF/B-VII.1+ SG34 <sup>239</sup> Pu .....	38
<b>7. Investigation on the prompt neutron fission spectrum of the <sup>239</sup>Pu .....</b>	<b>40</b>
7.1 Different <sup>239</sup> Pu spectra (PFNS) .....	40
7.2 Fast, intermediate and thermal flux experiments .....	41
7.3 Summary of the PFNS study .....	46
<b>8. Conclusions and recommendations .....</b>	<b>47</b>
<b>9. References .....</b>	<b>48</b>

### List of Figures

1: General strategy used in Subgroup 34 for the evaluation of <sup>239</sup> Pu resonance energy range .....	10
2: C/E results for Pu-SOL-THERM configurations based on ENDF/B-VII. 1 .....	11
3: C/E results for Pu-SOL-THERM configurations based on JEFF-3.1 [3] .....	12
4: Contribution of the external levels in the resonance region .....	15
5: Results of SAMMY fit of the total, fission and capture cross-section data .....	16
6: MCNP results for seven ICSBEP benchmarks listed in Table 3 .....	18
7: Cumulative Porter-Thomas integral distribution calculated with the neutron widths of the s-wave resonances observed below 1 keV .....	21
8: Relative uncertainties and correlation matrix for the total cross-section .....	22
9: Relative uncertainties and correlation matrix for the elastic cross-section .....	23



10: Relative uncertainties and correlation matrix for the capture cross-section .....	24
11: Relative uncertainties and correlation matrix for the fission cross-section.....	25
12: Cross-correlation matrix between the capture and elastic cross-sections .....	26
13: Cross-correlation matrix between the capture and fission cross-sections.....	27
14: Cross-correlation matrix between the fission and elastic cross-sections .....	28
15: Comparison of both the $^{239}\text{Pu}$ fission cross-section and the $(n,\gamma f)$ reaction deduced from the resonance parameters (upper plot) and calculated with the AVXSF code (lower plot) .....	30
16: Comparison of the $^{239}\text{Pu}$ prompt neutron multiplicity available in the JEFF libraries.....	31
17: The upper plot represents the neutron multiplicities calculated with and without the $(n,\gamma f)$ process.....	32
18: Average $(C/E-1)$ results obtained from the interpretation of the CERES-PU programme carried out in the DIMPLE reactor with the Monte Carlo code TRIPOLI.....	36
19: Fuel inventory calculations in PWR (ALIX-HBU program) for high burn-up between 65 GWd/t and 85 GWd/t .....	37
20: Residual reactivity effect obtained with JEFF-3.1.1 and JEFF-3.2 for various MOX configurations measured in the EOLE facility of CEA Cadarache.....	38
21: Kornilov spectrum, Maslov spectrum and other international evaluation file spectra compared to a Maxwellian distribution.....	41
22: $k_{\text{eff}}$ sensitivities on spectrum for ZONA2B and PU-MET-FAST 001 fast flux spectrum experiments .....	43
23: Fissile zone outgoing net current discrepancy between JEFF-3.1.1 and Kornilov spectra calculations.....	46

### List of Tables

1: PST Benchmarks and associated parameters.....	13
2: Thermal values and integral quantities calculated with SAMMY .....	17
3: ICSBEP benchmarks used in the $^{239}\text{Pu}$ evaluation.....	18
4: Relative uncertainties calculated for the total, capture, fission and elastic cross-sections.....	22
5: Values of the free parameters $v_i$ determined in this work and compared with those reported in [35] .....	33
6: Integral results (in pcm) obtained with the JEFF-3.1.1 and JEFF-3.1.1+SG34 $^{239}\text{Pu}$ libraries with the Monte Carlo code TRIPOLI-4.....	35
7: Value for the K1 parameter .....	36
8: Bias on the reactivity temperature coefficient (pcm/ $^{\circ}\text{C}$ ) calculated with APOLLO for the MISTRAL-3 programme carried out in the EOLE facility of Cadarache.....	37
9: Calculated $k_{\text{eff}}$ C/E values.....	38
10: First moment of energy distributions for all spectra.....	41
11: Criticality fast spectrum experiments – Difference between Maslov, Kornilov and JEFF-3.1.1 calculations.....	42
12: Mock-up fast spectrum experiments – Difference between Maslov, Kornilov and JEFF-3.1.1 calculations.....	42
13: Criticality intermediate spectrum experiments - Difference between Maslov, Kornilov and JEFF-3.1.1 calculations.....	43
14: Criticality thermal spectrum experiments - Difference between Maslov, Kornilov and JEFF-3.1.1 calculations.....	44
15: EOLE mock-up thermal spectrum experiments - Difference between Maslov, Kornilov and JEFF-3.1.1 calculations.....	44
16: PU-SOL-THERM-001 $k_{\infty}$ - JEFF-3.1.1 versus Kornilov calculations expressed in PCM.....	45

## 1. Introduction

In recent history, the United States and Europe have adopted the same evaluation for the  $^{239}\text{Pu}$  resonance region, largely based on work from the Oak Ridge National Laboratory (ORNL, USA) and the French Atomic Energy Commission (CEA Cadarache). In data testing for ENDF/B-VII.0, a general overprediction of Pu-SOL-THERMAL assemblies was noted, with an overprediction of typically about 0.5% - a very serious discrepancy indeed. Testing of the new evaluation in intermediate assemblies also shows a very large (and unwanted) increase in the  $C/E$ 's.

Concerning work done in recent years, two efforts should be mentioned. Firstly, the JEFF community has developed an updated  $^{239}\text{Pu}$  file for JEFF-3.1.1 with modifications to the original JEFF-3.1 file, at thermal energies, which has improved some of the above discrepancies. Secondly, at ORNL, Derrien and Leal have developed a new set of resonance parameters that has been incorporated into a file in ENDF/A for testing. This most recent evaluation is more consistent with the cross-section resonance data and is believed by evaluators to be the best representation of these data to date. Nonetheless, this new evaluation does not improve the poor integral performance of the ENDF/B-VII.0 file, and in fact most of the discrepancies become slightly worse, as noted by McKnight at the June 2009 CSEWG meeting.

The goal of this subgroup is to bring together the OECD/NEA experts in this area to further investigate if a new evaluation could be developed that uses the most accurate fundamental cross-section data with nuclear theory constraints, and also better predicts the relevant integral criticality data.

## 2. Tasks

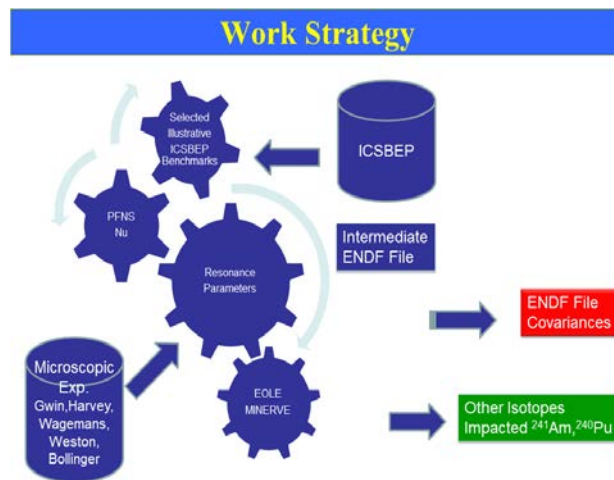
To obtain an improvement of  $^{239}\text{Pu}$  resonances both from microscopic and integral experiments points of view, several tasks were proposed at the beginning of this subgroup activity:

- Evaluation tasks:
  - $^{239}\text{Pu}$  resolved resonance range with covariances,
  - $^{239}\text{Pu}$  unresolved resonances range with covariances,
  - $^{239}\text{Pu}$  fission spectra ( $\chi$ ),
  - $^{239}\text{Pu}$  nu-bar in the thermal range as well as in the resonance range.
- Benchmarking tasks:
  - Define a set of public benchmarks related to  $^{239}\text{Pu}$  nuclear data: ICSBEP and IRPhEP,
  - Calculations of these benchmarks with various evaluations (ENDF, JEFF, JENDL, ...),
  - Spot as far as possible (via perturbation analysis) possible nuclear data improvements.

In addition, the subgroup considered various activities that might be related to  $^{239}\text{Pu}$ :

- Insure a proper link with Subgroup 32 on the unresolved treatment.
- Account for related activities:
  - LANL has done simulations to test the impact of various prompt neutron spectra on criticality, and found a significant sensitivity of the results to the  $\chi$  matrix adopted. Subgroup 34 should take advantage of the on-going work, co-ordinated by a new IAEA CRP, on the prompt fission neutron spectrum.
  - Fast region evaluations (JEFF, ENDF) and the corresponding partial cross-section splits: contributions from capture, inelastic, etc. are quite different and differences between various evaluations for inelastic scattering were stressed.
- Initiate or target new microscopic measurements if required.

The general strategy of this subgroup is synthesised in Figure 1.

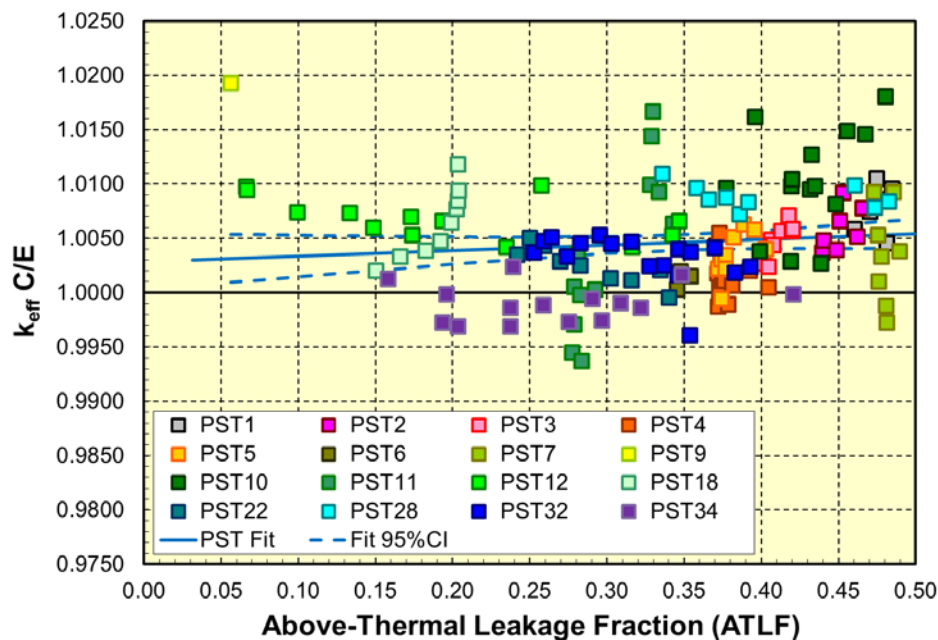
**Figure 1: General strategy used in Subgroup 34 for the evaluation of  $^{239}\text{Pu}$  resonance energy range**

### 3. Illustrative ICSEB benchmark: Description and initial results

#### 3.1 Initial result with ENDF library

An overprediction in calculated reactivity ( $k_{\text{eff}}$  for Pu fuelled systems, particularly thermal solution systems) has been an important issue for many years. This is illustrated in Figure 2, where the  $k_{\text{eff}}$  C/E results are displayed for a suite of over 150 International Criticality Safety Benchmark Evaluation Project (ICSBEP) Pu-SOL-THERM configurations [1].

Figure 2: C/E results for Pu-SOL-THERM configurations based on ENDF/B-VII. 1



These results were obtained using LANL's MCNP6.1 [2] continuous energy Monte Carlo code and ENDF/B-VII.1 cross-sections (.80c ACE files and the associated .20t thermal kernels). Similar results have been obtained in the past with other cross-section files such as JEFF-3.1.1 and JENDL-4.0.

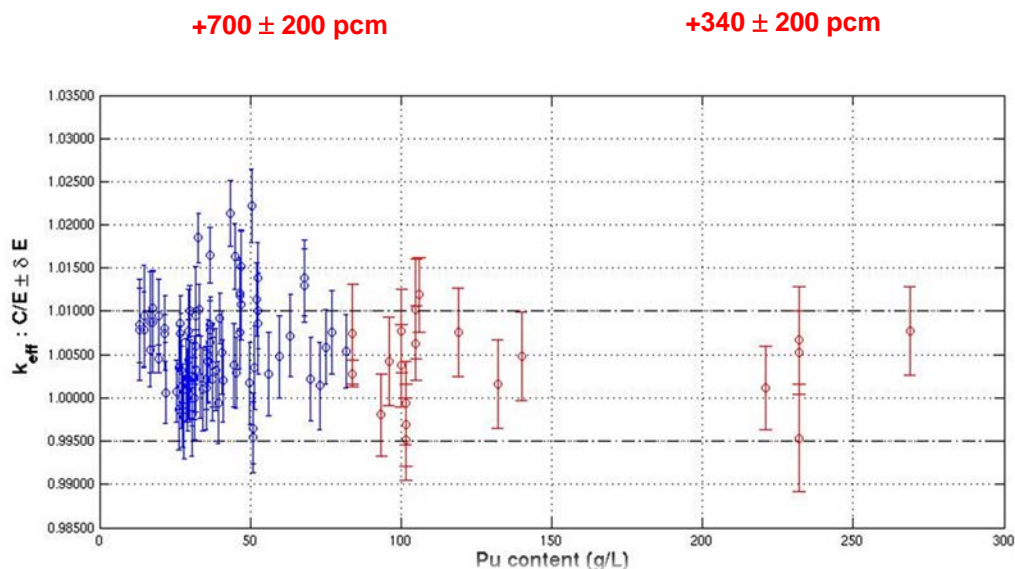
Figure 2 also illustrates a linear fit versus the abscissa's "Above Thermal Leakage Fraction" (ATLF). This parameter has been used in the past when calculating thermal solution of Highly Enriched Uranium (HEU) systems. If the benchmark measurements and underlying nuclear data are accurate, it can be expected that a regression equation will be obtained. In this equation, the intercept, or bias, term plus or minus its uncertainty should be unity and the slope, or trend, term plus or minus its uncertainty should be zero. The latter goal is attained, as the trend term and its 95% confidence interval for this fit is  $+0.0051 \pm 0.0073$  but there is evidence for a bias as the intercept term is  $1.0029 \pm 0.0026$ .

Similar fits can be made for  $k_{\text{eff}}$  C/E versus other parameters, including "Above Thermal Fission Fraction (ATFF)",  $^{239}\text{Pu}/\text{Pu}$  atom fraction, grams Pu/liter of solution or Hydrogen-to-Pu in solution ratio. Regression analyses generally yield intercept terms indicative of a 500 pcm or so bias.

### 3.2 Initial result with JEFF libraries (from JEFF-3.1 to JEFF-3.1.1)

It was noted in 2006 that for JEFF-3.1, ICSBEP/PU-SOL-THERM Benchmarks showed an overestimation of the  $k_{\text{eff}}$  prediction [3] [4]. Figure 3 presents some results on this issue for a limited set: PST001 to PST011 ( $^{240}\text{Pu}$  content < 4.8%) and PST012 ( $^{240}\text{Pu}$  content = 19%). This overestimation was between 340 and 700 pcm.

Figure 3: C/E results for Pu-SOL-THERM configurations based on JEFF-3.1 [3]



JEFF participants thus proposed a revised  $^{239}\text{Pu}$  evaluation showing a better overall integral behaviour regarding the PST suite. This evaluation was part of JEFF-3.1.1 library. As mentioned in JEFF Report 22 [5] and in [6], an overall remaining bias of around +250 pcm was found at that time with this latter JEFF version for Pu-Sol-Therm with Pu concentration < 80 g/l and around +50 pcm for Pu-Sol-Therm with Pu concentration >80 g/l. Additional benchmarks were evaluated on various 100% MOX experiments performed in EOLE since 1993, using the same MOX 7%Pu fuel pins. These successive MH1.2, MISTRAL2 and MISTRAL3 experiments were carried out respectively in 1993, 1997 and 1999. A remaining bias was spotted mainly due to  $^{241}\text{Am}$ .

### 3.3 Selected ICSBEP Pu-SOL-THERM set

As a new  $^{239}\text{Pu}$  evaluated nuclear data file will be available it is neither necessary nor practical to recalculate the reactivity for all critical configurations. To some extent, a small subset of these benchmarks has been selected whose attributes span the phase space defined by these parameters. The selected benchmarks are defined in Table 1.

**Table 1: PST Benchmarks and associated parameters**

<b>Benchmark name</b>	<b>Benchmark parameter</b>
PST12.13 – PST1.4	Above-Thermal Leakage Fraction (ATLF)
PST12.10 – PST34.14	Above-Thermal Fission Fraction (ATFF)
PST18.6 – PST4.1	<sup>239</sup> Pu/Pu Atom Percent (a/o)
PST12.10 – PST34.3	Grams Pu / Liter of Solution (g Pu/l)
PST34.14 – PST9	Hydrogen to Pu (H/Pu) in Solution

The average  $k_{\text{eff}}$  C/E for all PST benchmarks, calculated with ENDF/B-VII.1 cross-sections is 1.0046 while the average  $k_{\text{eff}}$  C/E for the 8 sample subset is 1.0058, confirming the assertion that this subset of benchmarks adequately represents the complete population.

## 4. Re-evaluation of the $^{239}\text{Pu}$ resolved resonance parameters in the energy range $10^{-5}$ eV to 2.5 keV

### 4.1 Introduction

A collaborative effort between the Oak Ridge National Laboratory (ORNL) and The French Atomic Energy Commission (CEA/Cadarache) was initiated under the auspices of the US Department of Energy and the Nuclear Energy Agency (NEA) to address issues pertinent to the performance of the  $^{239}\text{Pu}$  cross-sections in benchmark calculations. Researcher L. Leal (ORNL) worked with G. Noguere in Cadarache for two months on the analysis and evaluation of the  $^{239}\text{Pu}$  in the resolved resonance region. The following tasks were performed:

- use the SAMMY [7] code to perform resonance analysis using the best selected set of experimental time-of-flight data;
- generate cross-section library with the NJOY [8] code for use in benchmark calculations with the MCNP [2] code;
- generate cross-section library with the GALILEE (NJOY+CALENDF) code [9] for use in benchmark calculations with the TRIPOLI [10] and APOLLO [11] codes;
- use a selected set of experimental benchmarks with average of neutron lethargy causing fission spanning the energy range from 0.01 eV to 3 eV;
- use MISTRAL and FUBILA experiments (MOX fuel) performed at the EOLE facility to test the evaluation;
- evaluate nu-bar to improve benchmark results.

### 4.2 General descriptions

In the 1980s and early 1990s, H. Derrien and others [12] [13] performed a  $^{239}\text{Pu}$  evaluation in a collaborative work including CEA and ORNL. At that time, due to computer limitations for data storage and processing, the decision was made to split the resonance region in three parts, namely,  $10^{-5}$  eV to 1 keV, 1 keV to 2 keV, and 2 keV to 2.5 keV. The evaluation was accepted for inclusion in the ENDF and JEFF nuclear data libraries and is now included in the latest release of ENDF, the ENDF/B-VII.1 and also in the JEFF-3.1 libraries. While the evaluation was performed based on high-resolution data, mainly on transmission data [14] taken at the Oak Ridge Electron Linear Accelerator (ORELA) at ORNL, no benchmark testing was performed at the time the evaluation was released. Later benchmark calculations indicated deficiencies on the  $^{239}\text{Pu}$  evaluation in reproducing integral results. Also, some additional issues with the evaluation arose from the use of three distinct sets of resonance parameters. The cross-sections calculated at the energy boundary of two consecutive disjoint resonance parameter sets could be different, leading to discontinuity. Another concern relates to data uncertainty assessment using resonance parameter covariance. For data uncertainty analysis, the use of a single resonance parameter set covering the entire energy region would be preferable since the disjoint set of resonance parameters does not permit the determination of a full uncertainty correlation in the entire energy region. Hence, the decision was made to combine the three sets of resonance parameters and re-do the evaluation. The task was achieved thanks to a substantial improvement of computer resources. As a result, a resonance parameter evaluation was carried out by Derrien [15], covering the energy range  $10^{-5}$  eV to 2.5 keV. Nevertheless, the evaluation was unable to improve benchmark results. The evaluation was not proposed for inclusion in either the ENDF or the JEFF project.

To improve benchmark results, efforts were made by D. Bernard and others [16] at CEA/Cadarache to re-evaluate the  $^{239}\text{Pu}$  resonance parameters and nu-bar. Since the resonance evaluation for the whole energy



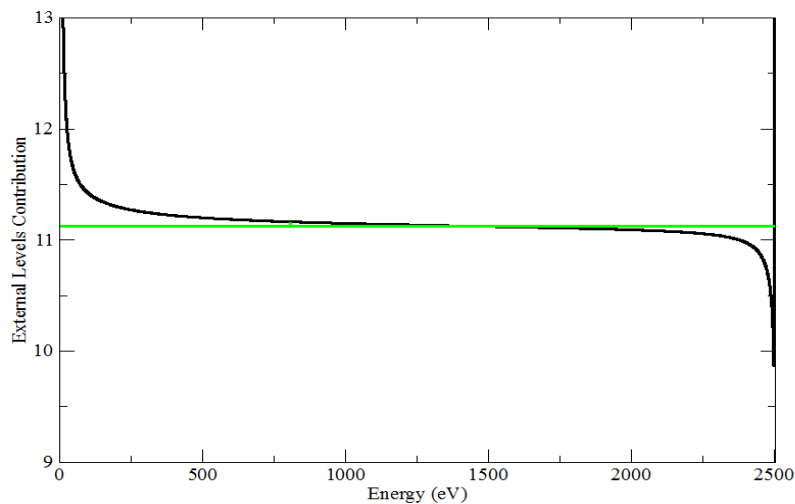
region was not available at the time, the work performed by Bernard was based on the JEFF-3.1 evaluation, i.e. with the three disjoint sets of resonance parameters. Bernard's evaluation improved the results of benchmark calculations significantly.

### 4.3 ORNL/CEA New <sup>239</sup>Pu Evaluation in the energy range 10<sup>-5</sup> eV to 2.5 keV

#### 4.3.1 Resonance parameter evaluation procedure

With the set of resonance parameters covering the energy region up to 2.5 keV a good set of external resonance parameters were determined. The technique used for deriving the external levels is described in [17]. Six resonance levels with negative energies and nine levels above 2.5 keV were sufficient to represent the external resonance interference effect in the energy region 10<sup>-5</sup> eV to 2.5 keV. The first negative level (close to zero) has a very small neutron width. It does not much contribute to the interference effect in the resonance region. However, it is used to get a representation in the shape of eta ( $\eta$ ) that bends down at very low energy [18]. Figure 4 shows the cross-section shape in the resonance region due only to the external energy resonance levels. It should be noted that the cross-section value converges to 11.13 barns, which represents the potential cross-section for <sup>239</sup>Pu determined with an effective scattering radius of 9.41 fm. This feature indicates that the external levels' contribution to the cross-section in the energy range 10<sup>-5</sup> eV to 2.5 keV is appropriate.

**Figure 4: Contribution of the external levels in the resonance region**



The experimental database used in the new evaluation is essentially the same as that used by Derrien [15]. However, information derived from the knowledge of benchmark calculation results was also included in the SAMMY analysis together with the fitting of the differential data. Two quantities were essential in determining the best set of resonance parameters that fitted the experimental differential data and in improving the benchmark results. The two quantities are  $\eta$  and the effective K1. These quantities are defined as:

$$\eta = \frac{v\sigma_f}{\sigma_a} = \frac{v}{1+\alpha} \quad , \quad (1)$$

where

$$\alpha = \frac{\sigma_\gamma}{\sigma_f} \quad ,$$

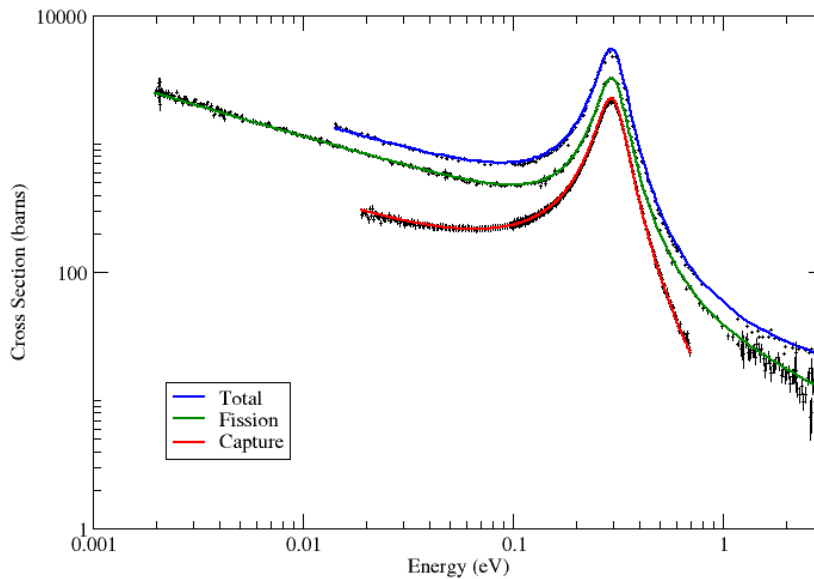
and

$$K1 = \overline{v\sigma_{0f}g_f} - \sigma_{0a}g_a \quad . \quad (2)$$

The cross-sections  $\sigma_{0f}$  and  $\sigma_{0a}$  are, respectively, the fission and absorption cross-sections at the thermal energy (0.0253 eV), whereas  $g_f$  and  $g_a$  are the Westcott's g-factors. The  $\bar{\nu}$  value at thermal energy is used in calculating the effective K1 from Equation (2). It was noted that the benchmark results were very sensitive to these two parameters. The benchmark results indicated that in some cases the sensitivity to K1 was more significant than to  $\eta$ . The K1 value for  $^{239}\text{Pu}$  is higher than that of other major isotopes. For instance, for  $^{235}\text{U}$  K1 value is around 722 barns whereas for  $^{239}\text{Pu}$  it is 1160 barns.

An example of the SAMMY fit of the experimental differential data is displayed in Figure 5 for the total cross-section of Bollinger [19], fission cross-section of Wagemans [20], and capture cross-section of Gwin [20] in the energy region from 0.01 eV to 3 eV.

**Figure 5: Results of SAMMY fit of the total, fission and capture cross-section data**



Values of the cross-section at thermal energy (0.0253 eV), fission Westcott factors, thermal  $\bar{\nu}$ , resonance integrals and K1 value are shown in Table 2. The unit for cross-sections, K1 and resonance integral is barns whereas the Westcott factor is dimensionless. Also, shown in Table 2 are the values listed in the Atlas of Neutron Resonance (ANR) [22], ENDF/B-VII.1 (same as JEFF-3.1), and the values calculated using Bernard's evaluation which is included in JEFF-3.1.1. The thermal cross-section values listed in the ANR were used in the SAMMY evaluation. The values listed in Table 2 were calculated with the SAMMY code.

**Table 2: Thermal values and integral quantities calculated with SAMMY**

Quantity	ANR	ENDF/B-VII.1 (JEFF-3.1)	JEFF-3.1.1	ORNL/CEA
$\sigma_\gamma$	269.3 ± 2.9	270.64	272.72	270.06
$\sigma_f$	748.1 ± 2.0	747.65	747.08	747.19
$g_f$	1.0553 ± 0.0013	1.0544	1.0495	1.0516
$g_a$	1.0770 ± 0.0030	1.0784	1.0750	1.0771
$\bar{\nu}$	2.879 ± 0.006	2.873	2.868	2.868
$I_\gamma$	180 ± 20	181.44	181.50	180.09
$I_f$	303 ± 10	302.60	303.58	309.09
$K1$	1177.25	1166.62	1156.35	1161.30

#### 4.3.2 Benchmark calculations

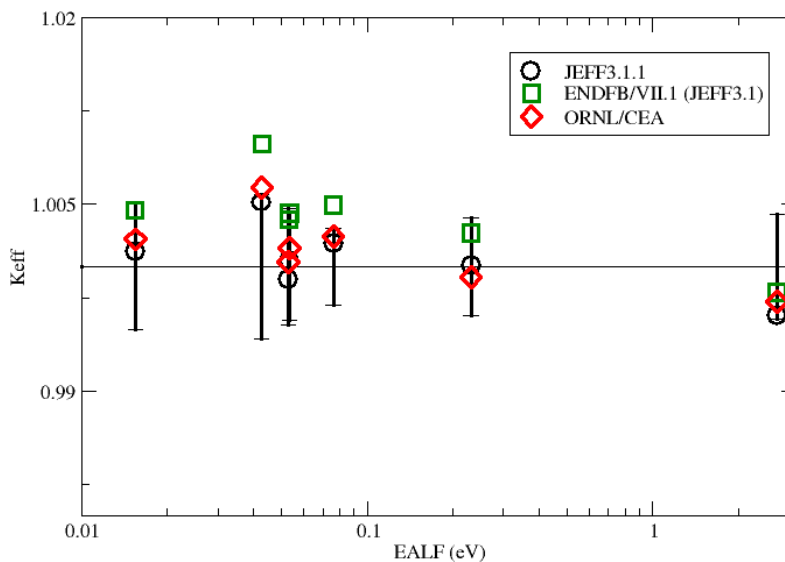
To verify the performance of the <sup>239</sup>Pu evaluation in benchmark calculations seven critical experiments were chosen from the International Criticality Safety Benchmark Evaluation Project (ICSBEP) in the International Handbook of Evaluated Criticality Safety Benchmark Experiments. These benchmark experiments consist of light water reflected spheres of plutonium nitrate solutions. The benchmarks, listed in Table 3, have the average of neutron lethargy causing fission (EALF) spanning the energy range of 0.01 eV to 3 eV. It should be noted that the uncertainty in these benchmarks are around 500 pcm.

Several resonance parameters were derived from the SAMMY fitting of the experimental differential data. Each time a resonance parameter was obtained with a satisfactory fitting of the differential data (a good chi-square), the SAMMY resonance parameter was converted in the ENDF format and inserted into the JEFF-3.1.1 by replacing the existing resonance parameter. The cross-section library created was then processed for use in Monte Carlo calculation using the MCNP code. The MCNP libraries were generated with the NJOY/ACER code. All the cross-section data for the remaining isotopes present in the benchmark experiments were taken from the ENDF/B-VII.0. The process from the SAMMY fitting of the experimental data to the MCNP calculation was automated, validated and tested.

**Table 3: ICSBEP benchmarks used in the <sup>239</sup>Pu evaluation**

Benchmark	Experimental $k_{\text{eff}}$	EALF (eV)
PU-SOL-THERM-001 case 4	$1.0000 \pm 0.0050$	0.0154
PU-SOL-THERM-004 case 1	$1.0000 \pm 0.0047$	0.0531
PU-SOL-THERM-012 case 10	$1.0000 \pm 0.0047$	0.0535
PU-SOL-THERM-012 case 13	$1.0000 \pm 0.0047$	0.0428
PU-SOL-THERM-018 case 6	$1.0000 \pm 0.0047$	0.0761
PU-SOL-THERM-034 case 4	$1.0000 \pm 0.0047$	0.231
PU-SOL-THERM-034 case 15	$1.0000 \pm 0.0047$	2.730

Various  $k_{\text{eff}}$  results were obtained for the seven benchmarks listed in Table 3. The impact of the cross-section change in the  $k_{\text{eff}}$  values was analysed and it was noted that a very minor change in the thermal cross-section and in the first resonance around 0.2956 eV would significantly change the  $k_{\text{eff}}$  value of the thermal benchmark listed in Table 3. In addition, results of sensitivity calculations using the TSUNAMI sequence of the SCALE code [23] indicated that, to achieve a reasonable  $k_{\text{eff}}$  result, a combined change on the nu-bar, on the fission and capture cross-sections values was needed as opposed to a simple change in one of these quantities alone. The very first attempt made was to focus on  $\eta$  (or  $\alpha$ ) since it involves these three quantities as indicated in Equation (1). However, further investigations indicated that the  $k_{\text{eff}}$  was also very sensitive to K1. Although no experimental measurement of K1 was found in the literature for <sup>239</sup>Pu integral experiments performed at the MINERVE could be used to infer the value of K1 which provided the best results for reactivity changes. A value of K1 around 1161 barns indicated that a reasonable  $k_{\text{eff}}$  could be achieved for the seven benchmarks listed in Table 3. Hence, in addition to fitting the experimental differential data SAMMY also fitted K1. The benchmark results for the seven benchmark displayed in Table 3 are shown in Figure 6.

**Figure 6: MCNP results for seven ICSBEP benchmarks listed in Table 3**

#### 4.4 Resonance Parameter Covariance Matrix (RPCM)

The Resonance Parameter Covariance Matrix established in the frame of this subgroup was generated with the marginalisation procedure of the CONRAD code [24]. The Governing equations and the results are given below.

##### 4.4.1 Governing equations

The marginalisation procedure of the CONRAD code is a mathematical technique designed to take into account experimental uncertainties of systematic origins in the uncertainty propagation calculations.

The neutron cross-section evaluation stands for a phenomenological description of a physical reality with a large number of parameters. Thousands of model parameters and experimental data points are needed to describe the main neutron reactions of interest for the nuclear applications. In practice, all of the model parameter covariances cannot be simultaneously estimated from well-defined sets of experimental data. The situation becomes more and more complex when the number of open reaction channels increases. This optimisation problem is non-convex in general, making it difficult to find the global optima.

A solution to simplify the problem consists in dividing the model parameter sequence into blocks of variables whose uncertainties can be propagated through fixed-order sequential data assimilation procedures. According to definitions and nomenclature used in statistics, we can identify the “observable,” “latent,” and “nuisance” variables. Observable variables can be directly determined from the experimental data. Latent variables as opposed to observable variables may define redundant parameters or hidden variables that cannot be observed directly. This term reflects the fact that such variables are really there, but they cannot be observed or measured for practical reasons. Nuisance variables, i.e. experimental corrections, correspond to the aspect of physical realities whose properties are not of particular interest as such but are fundamental in assessing reliable model parameters. As shown in [25-27], marginalisation techniques may provide appropriate solutions to propagate the nuisance and latent model parameters.

Here, only the uncertainty propagation of the observed and nuisance parameters is discussed. Therefore, the model parameters and the corresponding covariance matrix can be partitioned as:

$$\mu = \begin{pmatrix} x \\ \theta \end{pmatrix}, \quad \Sigma = \begin{pmatrix} \Sigma_{11} & \Sigma_{12} \\ \Sigma_{21} & \Sigma_{22} \end{pmatrix},$$

In which  $x=(x_1 \dots x_n)^T$  and  $\theta=(\theta_1 \dots \theta_m)^T$  represent the observable parameter and nuisance parameters, respectively. In the resonance range of the neutron cross-sections,  $x_i$  are the resonance parameters and  $\Sigma_{11}$  stands for the Resonance Parameter Covariance Matrix (RPCM). The matrix  $\Sigma_{22}$  contains the variances and covariances of the nuisance parameters. The marginalisation procedure can be mathematically expressed as follows:

$$\Sigma_{11} = M_x + H_\theta,$$

where

$$H_\theta = (G_x^T G_x)^{-1} G_x^T G_\theta \Sigma_{22} G_\theta^T G_x (G_x^T G_x)^{-1}.$$

The matrix  $M_x$  is the posterior covariance matrix obtained at the end of the fitting procedure. The derivative matrices  $G_x$  and  $G_\theta$  of the quantity  $z$  (reaction yield, transmission or neutron cross-section) to the parameter  $x$  and  $\theta$  are defined as:

$$G_x = \begin{pmatrix} \frac{\partial z_1}{\partial x_1} & \dots & \frac{\partial z_1}{\partial x_n} \\ \vdots & \ddots & \vdots \\ \frac{\partial z_k}{\partial x_1} & \dots & \frac{\partial z_k}{\partial x_n} \end{pmatrix},$$

and

$$G_\theta = \begin{pmatrix} \frac{\partial z_1}{\partial \theta_1} & \dots & \frac{\partial z_1}{\partial \theta_n} \\ \vdots & \ddots & \vdots \\ \frac{\partial z_k}{\partial \theta_1} & \dots & \frac{\partial z_k}{\partial \theta_n} \end{pmatrix}.$$

A two-step CONRAD calculation is needed to obtain the covariance matrices  $M_x$  and  $H_\theta$ . The first step consists in using the fitting procedure of CONRAD in order to determine  $M_x$  from well-defined sets of experimental data  $z$  of general dimension  $k$ . The second step consists in determining elements of  $H_\theta$  by calculating the derivative matrices  $G_x$  and  $G_\theta$ .

#### 4.4.2 CONRAD results

For practical applications, the marginalisation procedure was applied in the frame of a retroactive analysis. The latter analysis consists in calculating the covariances between the resonance parameters without changing their values. This can be achieved by replacing the experimental data with theoretical cross-sections. In this work, the retroactive analysis was applied on the fission and capture cross-sections.

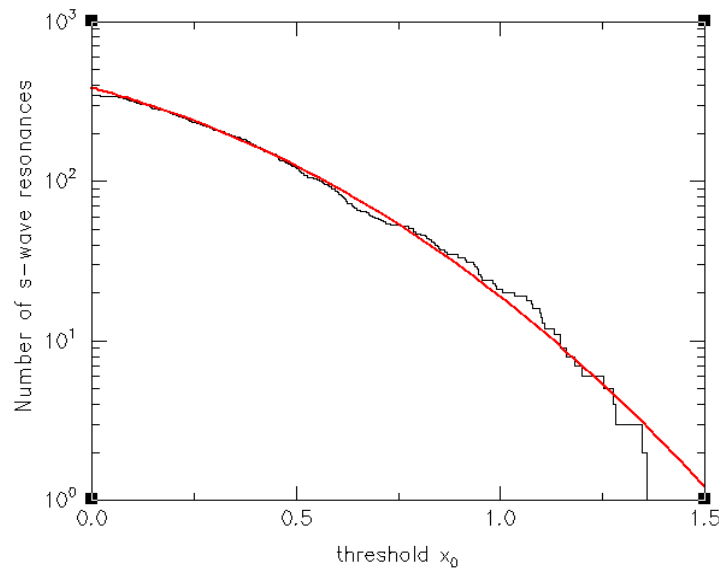
The number of s-wave resonances established in this work is 1043. In order to overcome problems related to storage and processing of large RPCM, a neutron width selection was applied to reduce the size of the resonance parameter set. The selection principle relies on properties of the cumulative Porter-Thomas integral distribution. Figure 7 represents the histogram of the reduced neutron width divided by its mean value. The abscise  $x_0$  is defined as:

$$x_0 = \frac{g\Gamma_n^0}{\langle g\Gamma_n^0 \rangle},$$

where  $g$  is the statistical spin factor. The smooth curve is given by:

$$N(x_0) = \text{Nerfc} \left( \sqrt{\frac{x_0}{2}} \right).$$

**Figure 7: Cumulative Porter-Thomas integral distribution calculated with the neutron widths of the s-wave resonances observed below 1 keV**



At  $x_0=0$ , the number of s-wave resonances is equal to:

$$N = \frac{E_{\max} - E_{\min}}{D_0} + 1,$$

Where  $E_{\min}$  and  $E_{\max}$  define the lower and upper energy limit of the energy range of interest and  $D_0$  is the s-wave mean level spacing. For <sup>239</sup>Pu, the energy limits are  $E_{\min}=0.3$  eV and  $E_{\max}=2.5$  keV.

An s-wave resonance is included in the marginalisation procedure if its reduced neutron width amplitude is larger than a threshold  $x_0$ . The latter threshold should fulfil the conditions  $\sigma_{\gamma,g}(x_0=0) \approx \sigma_{\gamma,g}(x_0>0)$  for the capture cross-section and  $\sigma_{f,g}(x_0=0) \approx \sigma_{f,g}(x_0>0)$  for the fission cross-section in a given energy group  $g$ . In this work, a broad energy mesh was used. This arbitrary choice allows removing three quarters of the s-wave resonances from the retroactive analysis. The final number of resonances is 302.

The energy domain was divided into three energy ranges to cover the thermal range, the first resonance at 0.3 eV and the resonance integral above 0.5 eV up to 2.5 keV. The final RPCM generated by CONRAD was converted into ENDF-6 format (MF=32, MT=151) and processed with the NJOY code. Results are shown in Figures 8 to 14. Table 4 reports the relative uncertainties for the total, fission, capture and elastic cross-sections.

In the RRR, the relative uncertainties for the fission and capture cross-sections remain below 3% and 7% respectively. The systematic uncertainties are the dominant components of the final uncertainties. Consequently, simple correlation structures are obtained. The present results were included in the latest NEA library JEFF-3.2.

**Table 4: Relative uncertainties calculated for the total, capture, fission and elastic cross-sections**

Energy Range (eV)	Total cross-section	Capture cross-section	Fission cross-section	Elastic cross-section
E < 0.1	1.4 %	4.2 %	0.9 %	4.6 %
0.1 – 0.54	1.9 %	4.2 %	1.9 %	3.7 %
0.54 – 4.0	1.3 %	3.6 %	1.1 %	4.2 %
4.0 – 22.6	3.1 %	7.1 %	3.0 %	3.3 %
22.6 – 454.0	3.9 %	6.5 %	3.5 %	5.7 %
454.0 – 2500.0	3.2 %	5.1 %	3.2 %	4.0 %

**Figure 8: Relative uncertainties and correlation matrix for the total cross-section**

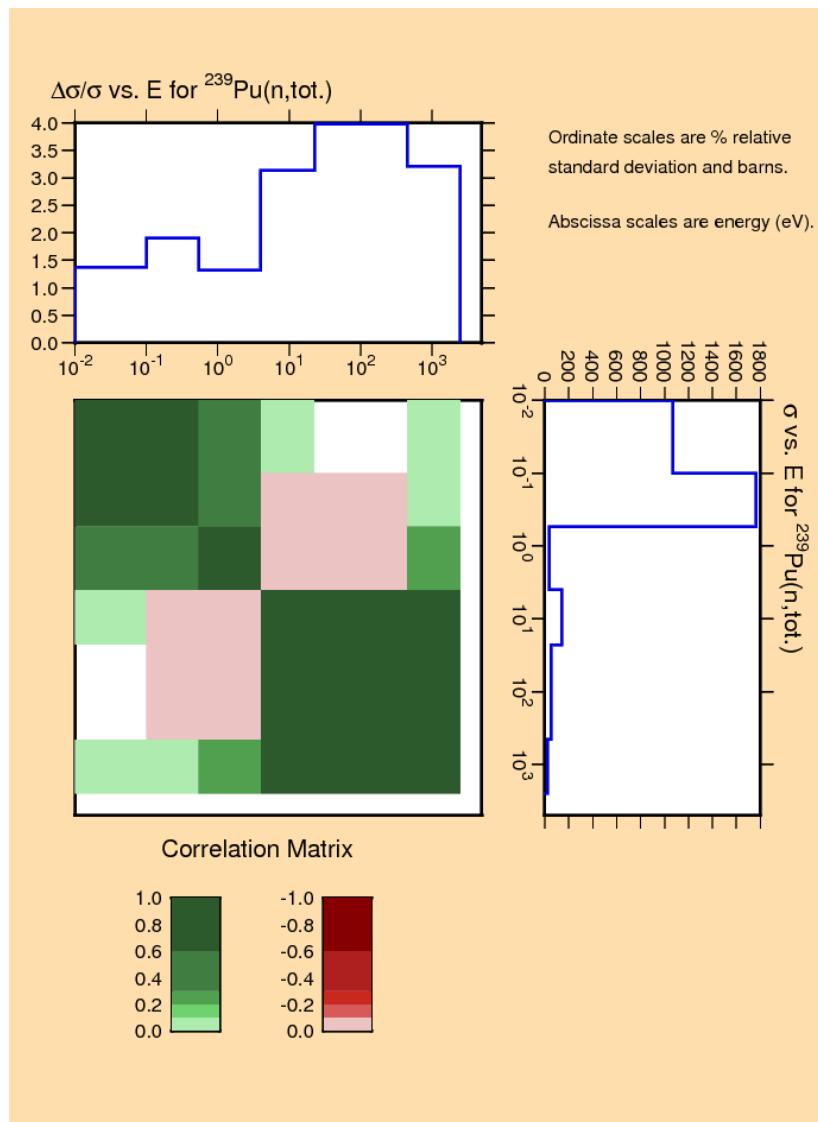




**Figure 9: Relative uncertainties and correlation matrix for the elastic cross-section**

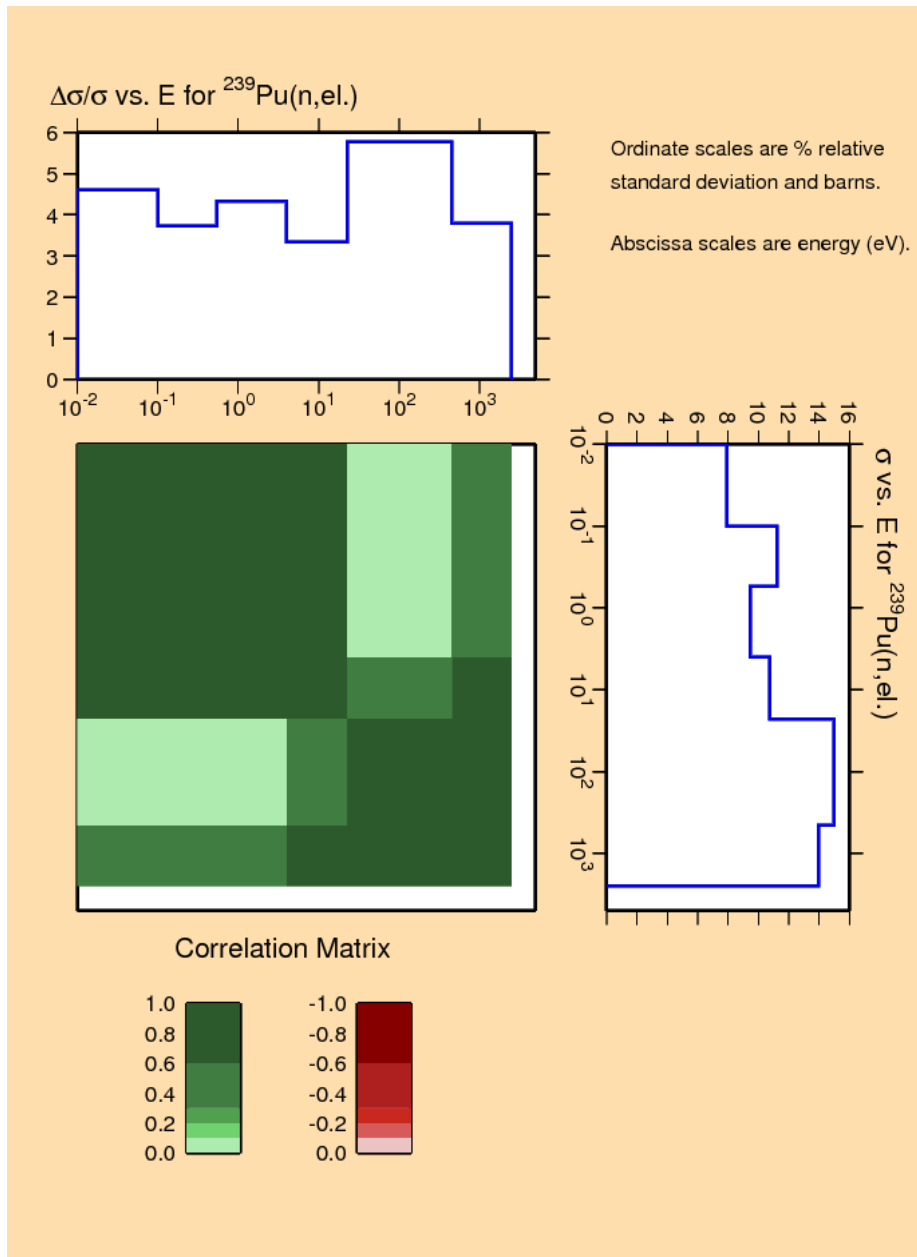


**Figure 10: Relative uncertainties and correlation matrix for the capture cross-section**

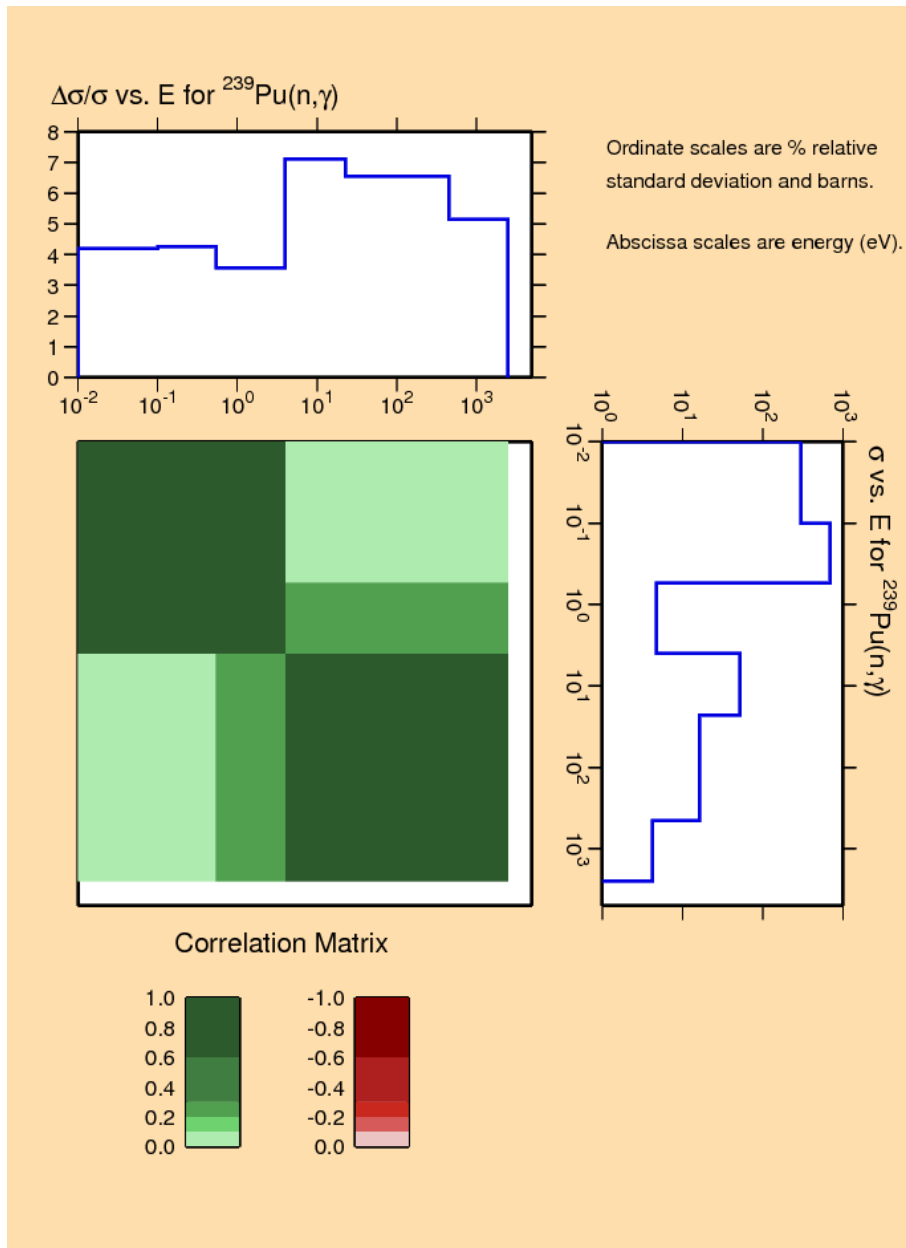


Figure 11: Relative uncertainties and correlation matrix for the fission cross-section

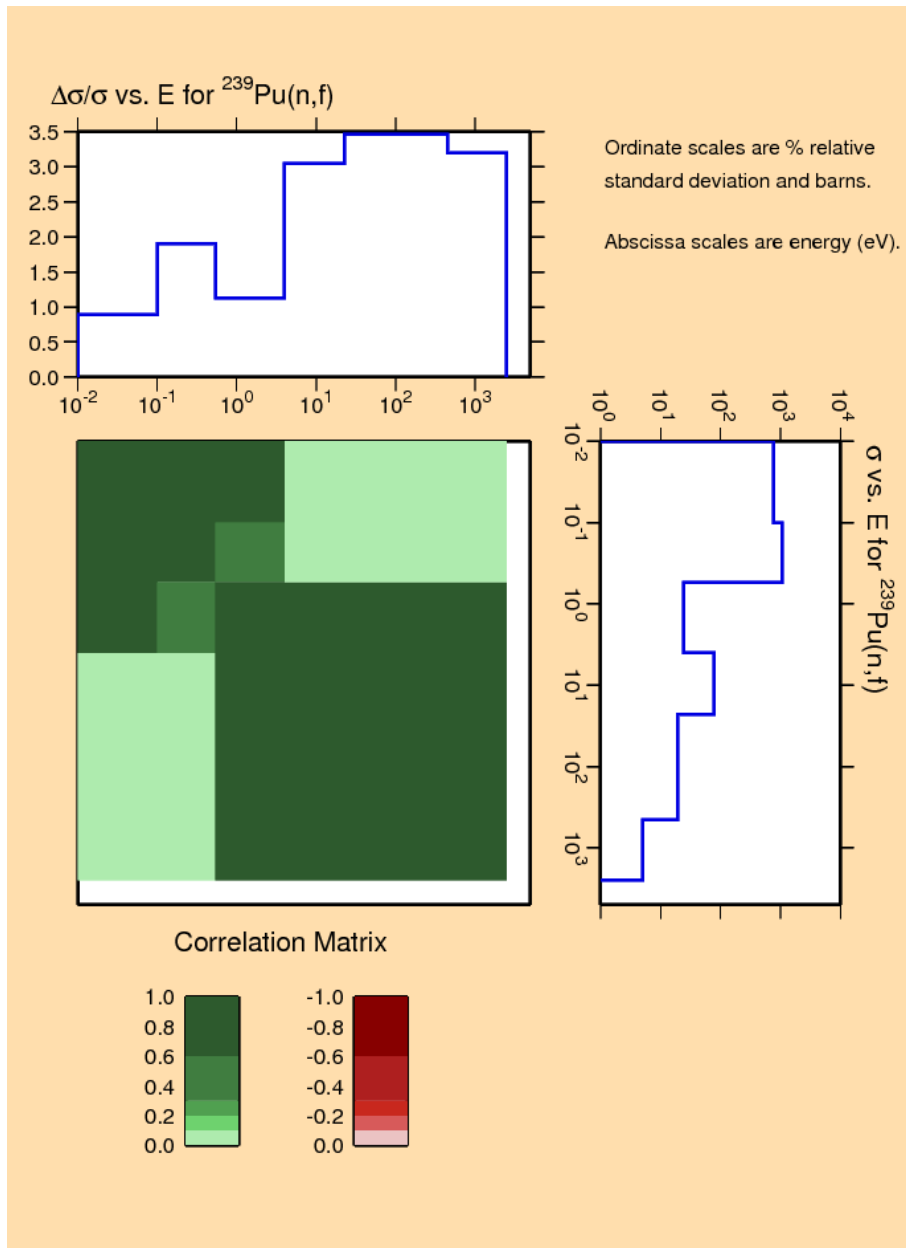


Figure 12: Cross-correlation matrix between the capture and elastic cross-sections

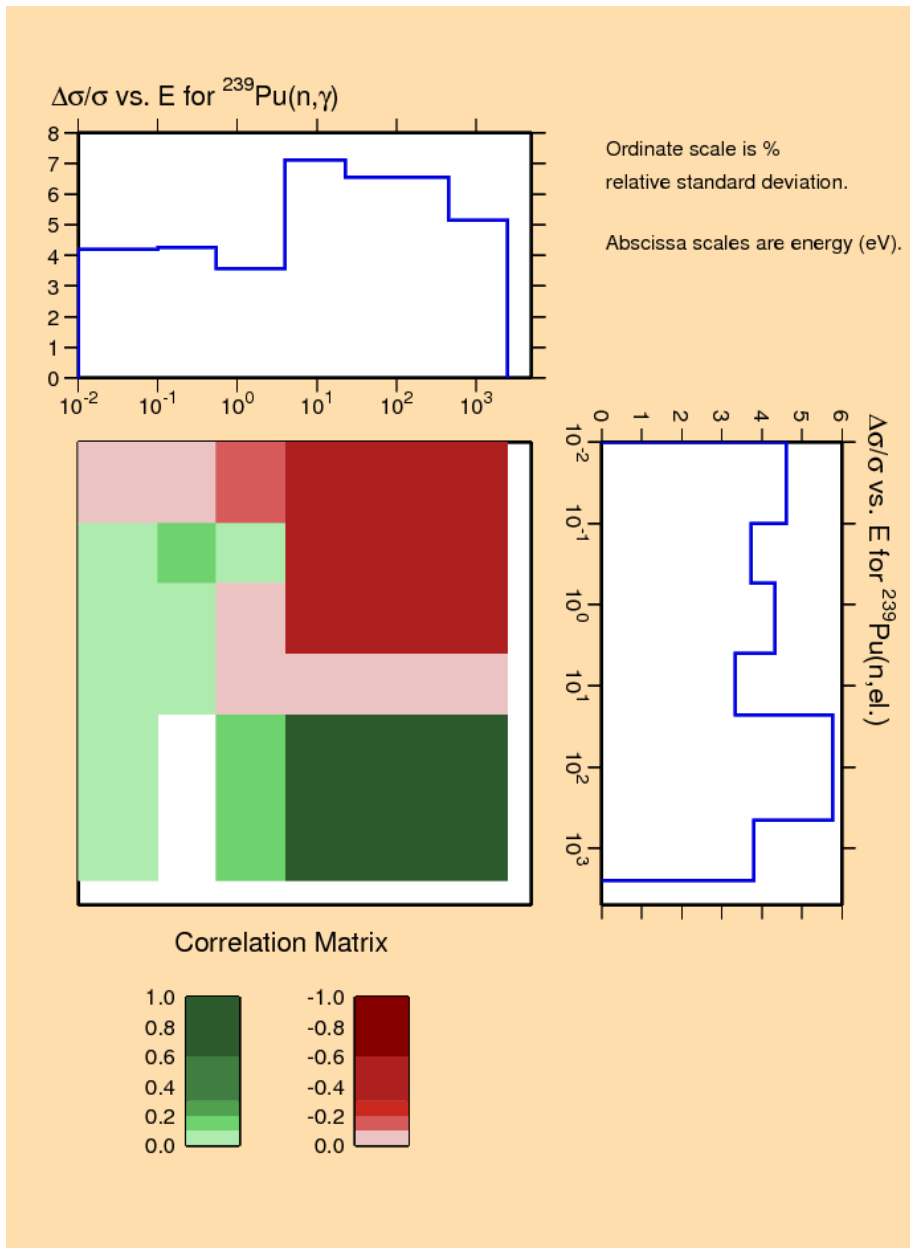
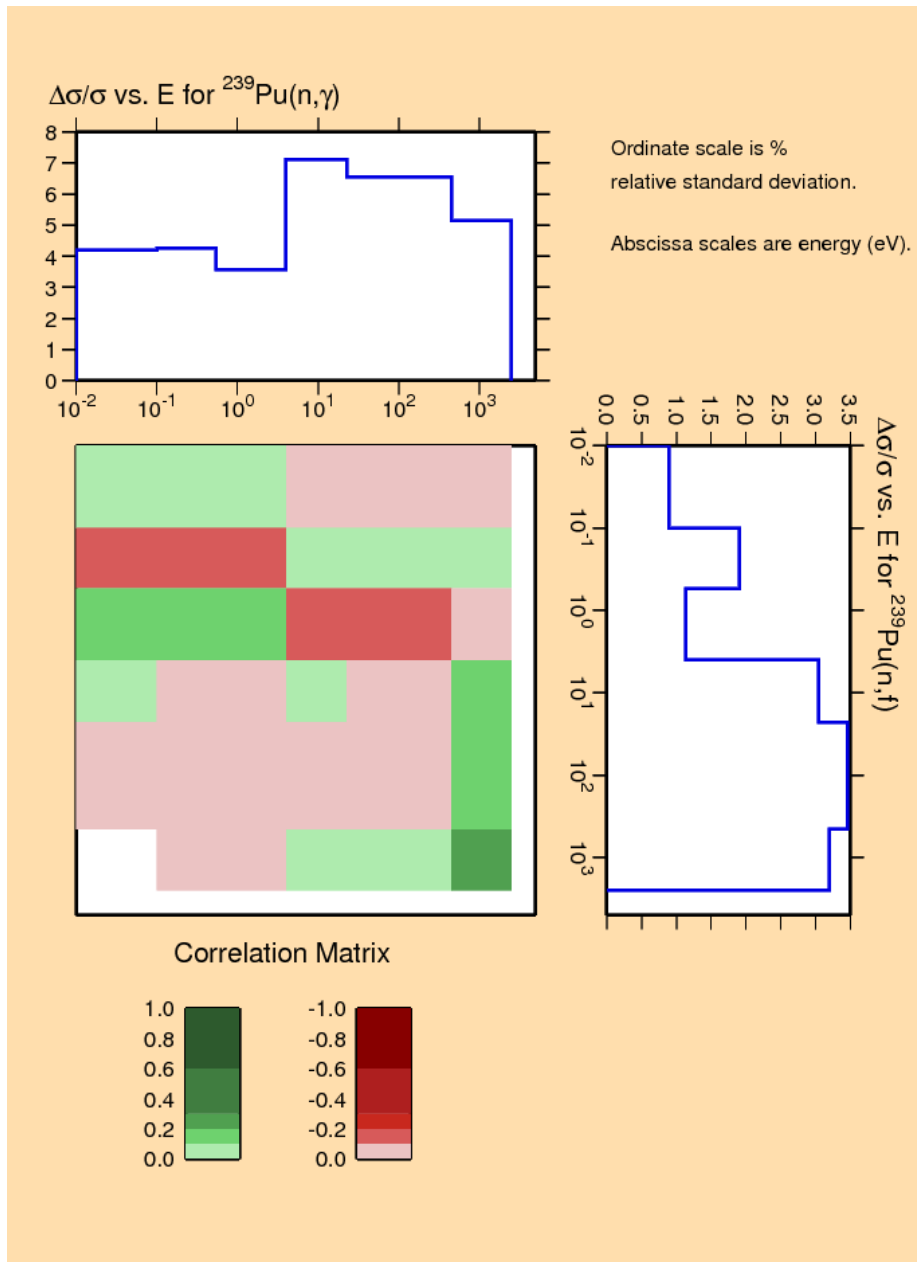
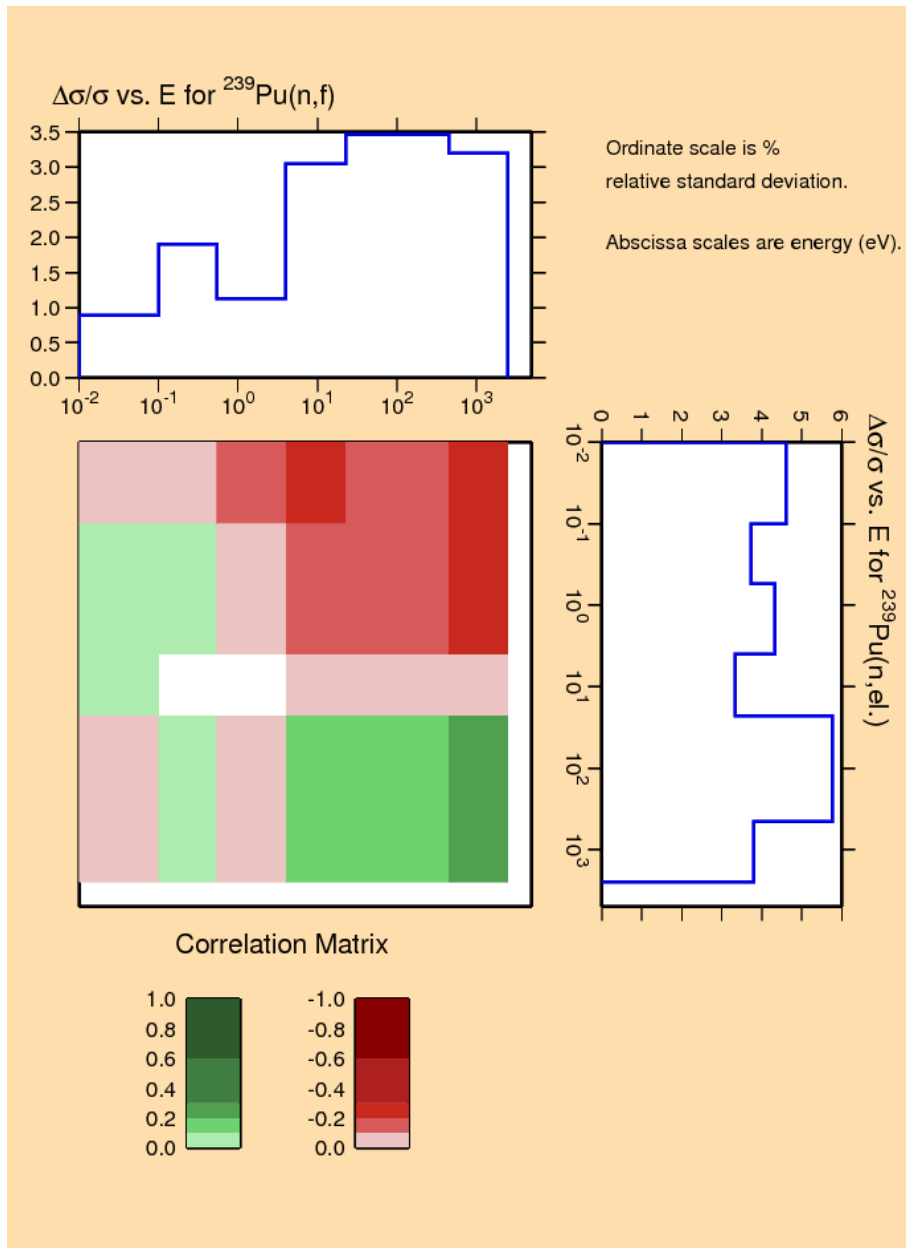


Figure 13: Cross-correlation matrix between the capture and fission cross-sections



**Figure 14: Cross-correlation matrix between the fission and elastic cross-sections**



## 5. Prompt neutron multiplicity in the resonance range

Large fluctuations of the neutron multiplicity were observed in the resonance range. According to the spin assignment, the observed fluctuations are stronger for resonances having  $J=1^+$ . The latter channel is characterised by an average fission width of about 30 meV, while for  $J=0^+$ , the average fission width is close to 2 eV since the number of fission transition states involved is larger (2 to 3 compared to 1 at low energy for the other s-wave resonance spin  $J=1^+$ ). The (n, $\gamma$ f) two-step reaction was introduced as a competitive reaction to explain the specific channel spin dependence observed in the prompt neutron multiplicity  $\nu_p(E)$ . The (n, $\gamma$ f) reaction and its implications are presented in this section.

### 5.1 Investigation of the two-step (n, $\gamma$ f) process

The (n, $\gamma$ f) process was emphasised by Lynn in 1959. The formal description of such a two-step process was published in 1965 in [28] and it was recalled in 1980 in [29]. Three PhD thesis performed on  $^{239}\text{Pu}$  provide additional results about this two-step process [30-32]. However, the existence of the (n, $\gamma$ f) reaction is still a topic of discussion because direct measurements of this reaction are a genuine challenge.

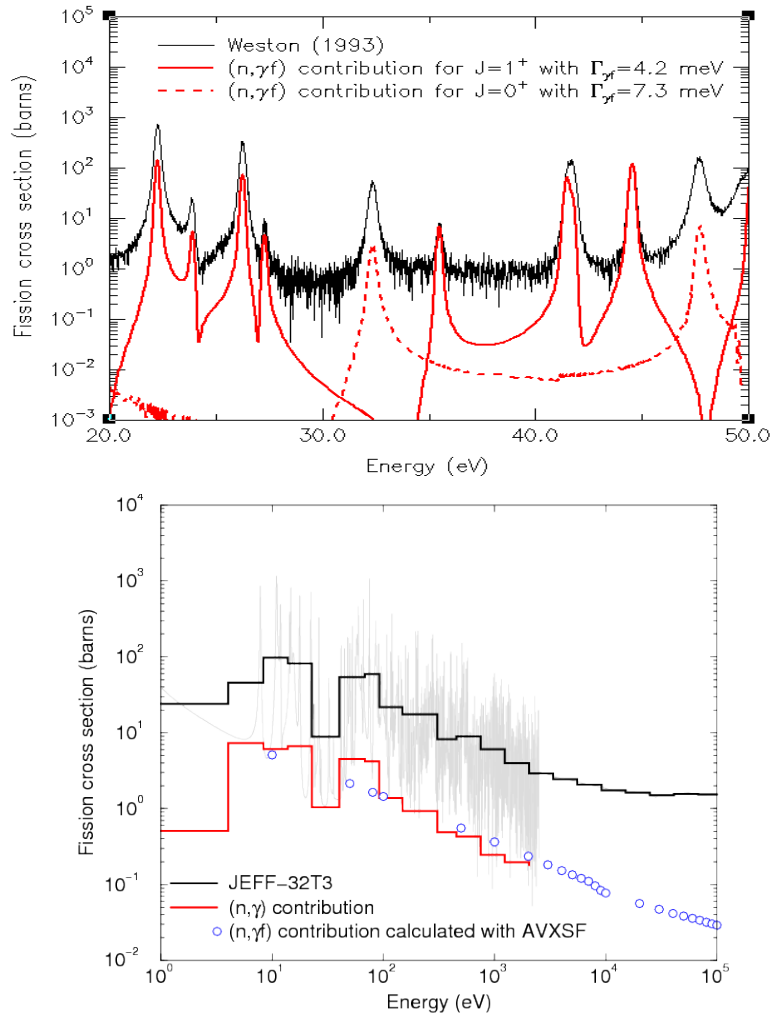
Authors that argue the existence of the (n, $\gamma$ f) process assume that the observed fission is the sum of the one-step (or “direct”) fission and of the two-step (n, $\gamma$ f) reaction:

$$\sigma_f^{obs}(E) = \sigma_f(E) + \sigma_{\gamma f}(E).$$

From a theoretical point of view, the (n,f) and (n, $\gamma$ f) reaction widths have to be fitted simultaneously during the Neutron Resonance Shape Analysis. Such an approach implies a modification of the resolved resonance range (RRR) formalism used in standard shape analysis codes (as SAMMY, REFIT, CONRAD...) and of the subsequent processing codes (as NJOY, CALENDF...). This work does not correspond to the present subgroup tasks. The alternative chosen in the present work was to deduce the contribution of two-step processes from the fitted Reich-Moore parameters by introducing additional J-dependent partial widths  $\Gamma_{\gamma f}$ . Due to the numerous intermediate states reached by gamma decays before second-step fission, the partial width of each spin J for the (n, $\gamma$ f) reaction can be assumed constant below 2.5 keV.

Figure 15 shows the contribution of this competitive reaction in the RRR and in the neutron spectroscopy continuum domain. Below 2.5 keV, we use  $\Gamma_{\gamma f} = 7.3$  meV for  $J=0^+$  and  $\Gamma_{\gamma f} = 4.2$  meV for  $J=1^+$ . The magnitude of the (n, $\gamma$ f) contribution deduced from the resonance parameters is compared with the theoretical curve estimated with the AVXSF code [33]. The latter code has been developed at Los Alamos by Eric Lynn since the early 1970s and a more robust and extensive version in Fortran 95 is now supported by CEA at Cadarache. Detailed formulae implemented in this nuclear fission data evaluation code that were in particular used for estimating the average cross-sections of the Pu family over the URR range up to 5.5 MeV can be found in [34].

**Figure 15: Comparison of both the  $^{239}\text{Pu}$  fission cross-section and the  $(n,\gamma f)$  reaction deduced from the resonance parameters (upper plot) and calculated with the AVXSF code (lower plot)**



Note: The JEFF-3.2T3 (=JEFF-3.2) evaluation contains the resonance parameters evaluated in the frame of this subgroup.

The upper plot of Figure 15 confirms the non-negligible contribution of the  $(n,\gamma f)$  reaction for small s-wave resonances having  $J=1^+$  because of the low one-step fission cross-section in that channel spin. Future evaluation works on  $^{239}\text{Pu}$  will have to include explicitly in the evaluated data file the two-step  $(n,\gamma f)$  reaction as an additional dedicated partial reaction width,  $\Gamma_{\gamma f}$ . The usual fitted fission width will be the one-step fission component only.

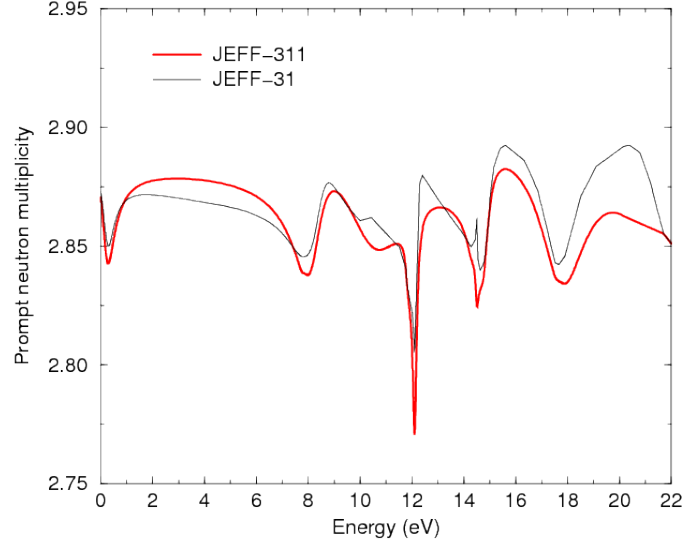
## 5.2 Study of the channel spin dependence of $\nu_p(E)$

As shown in the upper plot of Figure 15, the  $(n,\gamma f)$  reaction may become the dominant fission contribution for small resonances characterised by an angular momentum  $J=1^+$ . These properties were used to explain the large fluctuations of the prompt neutron multiplicity in the resonance range since the average energy carried away by the pre-fission photon is around 1 MeV; energy amount that is not available for the neutron emission during the fission process. The emitted number of neutrons is logically reduced in proportion. In the present work, we use a phenomenological decomposition of the neutron multiplicity. This decomposition was already applied by Eric Fort to establish the neutron multiplicity file released in the JEFF-3.1



library [35]. The low energy part (below 22 eV) was modified in the JEFF-3.1.1 library for improving the  $k_{\text{eff}}$  results of various benchmarks [4]. The JEFF-3.1.1 and JEFF-3.1 multiplicities are compared in Figure 16.

**Figure 16: Comparison of the  $^{239}\text{Pu}$  prompt neutron multiplicity available in the JEFF libraries**



Neutron multiplicity can be viewed as the sum of four contributions due to two fission widths  $\Gamma_f$  and  $\Gamma_{\gamma f}$  for each channel  $J=0$  and  $J=1$ . Neutron multiplicity can be expressed as follows:

$$\nu_p(E) \approx \sum_{i=1}^4 \nu_i P_i(E)$$

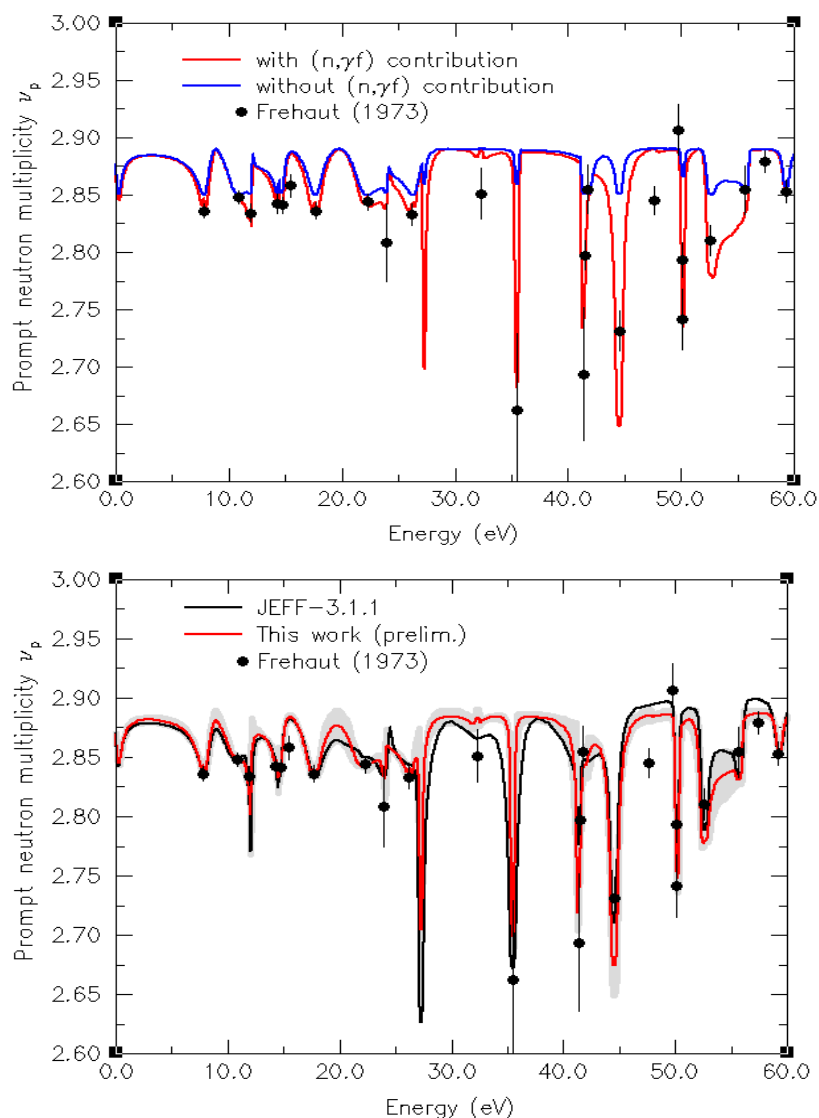
In which  $\nu_i$  are free parameters and  $P_i(E)$  are probabilities defined as:

$$P_i(E) = \frac{\sigma_i(E)}{\sigma_f(E) + \sigma_{\gamma f}(E)},$$

where  $\sigma_i(E)$  represents the partial one-step fission or  $(n,\gamma f)$  cross-sections for a given  $J$ .

Final results are shown in Figure 17. They were obtained using the CONRAD code involving a least-squared fit performed over EXFOR data [32] [36]. The theoretical curve was calculated with  $\Gamma_{\gamma f} = 7.3$  meV for  $J=0^+$  and  $\Gamma_{\gamma f} = 4.2$  meV for  $J=1^+$ .

Figure 17: The upper plot represents the neutron multiplicities calculated with and without the (n, $\gamma$ f) process



Note: The lower plot compares the present work with the JEFF-3.1.1 evaluation.

The upper plot compares the magnitude of neutron multiplicity with and without the contribution of the two-step (n, $\gamma$ f) process. Without the (n, $\gamma$ f) contribution, the phenomenological description of neutron multiplicity fails to reproduce the large variations observed for resonances having  $J=1$ . For  $J=0$ , the contribution of the (n, $\gamma$ f) reaction ( $\Gamma_{\gamma f} = 7.3$  meV) is negligible compared to the magnitude of the average one-step fission width as large as 2 eV.

The lower plot of Figure 17 shows that the present work is in good agreement with the JEFF-3.1.1 evaluation. The free parameters  $\nu_i$  extracted by CONRAD are reported in Table 5. The CONRAD results confirm the values reported in [35]. As a consequence, the neutron multiplicity energy shape in the resolved resonance range of JEFF-3.1.1 is recommended for the next  $^{239}\text{Pu}$  evaluation.

**Table 5: Values of the free parameters  $\nu_i$  determined in this work and compared with those reported in [35]**

Reaction	$J^\pi$	Fort et al. (1988)	This work
(n,f)	1 <sup>+</sup>	2.86	2.85
(n,f)	0 <sup>+</sup>	2.88	2.89
(n, $\gamma$ f)	1 <sup>+</sup>	2.66	2.62
(n, $\gamma$ f)	0 <sup>+</sup>	2.80	2.62

## 6. Integral validation of the $^{239}\text{Pu}$ resolved resonance range

Preliminary MCNP calculations on seven dedicated benchmarks were continuously performed during the elaboration of the resolved resonances with the SAMMY code. Results are reported in Section 4.3.2. Additional integral results are presented in this section based on both ENDF/B-VII.1 and JEFF-3.1.1 libraries as reference, i.e. the SG34  $^{239}\text{Pu}$  file replaces the existing ENDF and JEFF  $^{239}\text{Pu}$  files. The SG34  $^{239}\text{Pu}$  file contains new resonance parameters, nu-bar and  $(n,\gamma f)$  cross-section.

### 6.1 Integral validation based on JEFF-3.1.1 + SG34 $^{239}\text{Pu}$

The calculations were performed with the Monte Carlo code TRIPOLI. The resolved resonances established in the frame of this subgroup were included in the latest version of the NEA library JEFF-3.1.2 (=JEFF-3.1.1). The benchmarks of interest come from the ICSBEP and CEA databases.

#### 6.1.1 Plutonium Solution Thermal (ICSBEP)

The ICSBEP benchmarks of interest for this work are reported in Table 6. As indicated in Section 4.3.2, the benchmarks PST-001 and PST-004 consist of light water reflected spheres of plutonium nitrate solutions. The latest benchmark PST-016 has a cylindrical geometry. Results for two benchmarks (PST-001.4 and PST-004.1) have already been reported in Figure 6.

The mean value of the results seems to indicate a slight improvement of 50 pcm by using the new SG34  $^{239}\text{Pu}$  evaluation. This improvement is probably not significant because of the large statistical error of about 30 pcm on the TRIPOLI results. Therefore, the major conclusion provided by these results is that the performances of the new  $^{239}\text{Pu}$  evaluation will be equivalent to JEFF-3.1.1 for light water reactor applications. This conclusion is confirmed by the trends reported in Figure 6, where the red symbols are closer to the black circles obtained with the  $^{239}\text{Pu}$  evaluation of JEFF-3.1.1.

**Table 6: Integral results (in pcm) obtained with the JEFF-3.1.1 and JEFF-3.1.1+SG34 <sup>239</sup>Pu libraries with the Monte Carlo code TRIPOLI-4**

Benchmarks	series	Exp. Unc.	JEFF-3.1.1	JEFF-3.1.1+SG34 <sup>239</sup> Pu	Δ(SG34-JEFF-3.1.1)
<b>PU-SOL-THERM-001</b>	1	± 500	181 ± 36	150 ± 35	-31
	2		399 ± 35	339 ± 36	-60
	3		725 ± 35	656 ± 35	-69
	4		173 ± 35	89 ± 34	-84
	5		535 ± 35	470 ± 34	-65
	6		738 ± 34	698 ± 35	-40
<b>PU-SOL-THERM-004</b>	1	± 470	-332 ± 34	-333 ± 35	-1
	2		-503 ± 34	-498 ± 36	+5
	3		-356 ± 34	-258 ± 34	+98
	5		-413 ± 35	-422 ± 35	-9
	6		-184 ± 35	-180 ± 35	+4
	8		-252 ± 36	-300 ± 35	-48
<b>PU-SOL-THERM-016</b>	1	± 430	534 ± 28	450 ± 28	-84
	2		573 ± 28	504 ± 28	-69
	3		643 ± 28	594 ± 28	-49
	4		669 ± 27	553 ± 28	-116
	5		418 ± 28	258 ± 28	-160
	6		497 ± 29	413 ± 28	-84
	7		475 ± 28	429 ± 28	-46
Mean value			+238	+190	-48
Standard deviation			433	398	

Note: The results in red correspond to the benchmarks used during the Neutron Resonance Shape Analysis (see Section 4.3.2).

### 6.1.2 Mock-up facilities and power reactors.

The impact of the new <sup>239</sup>Pu evaluation was investigated with integral results obtained on mock-up facilities and power reactors by inserting the SG34 <sup>239</sup>Pu file in the JEFF-3.2 Test library, which also contains a new <sup>241</sup>Am evaluation in the resonance region.

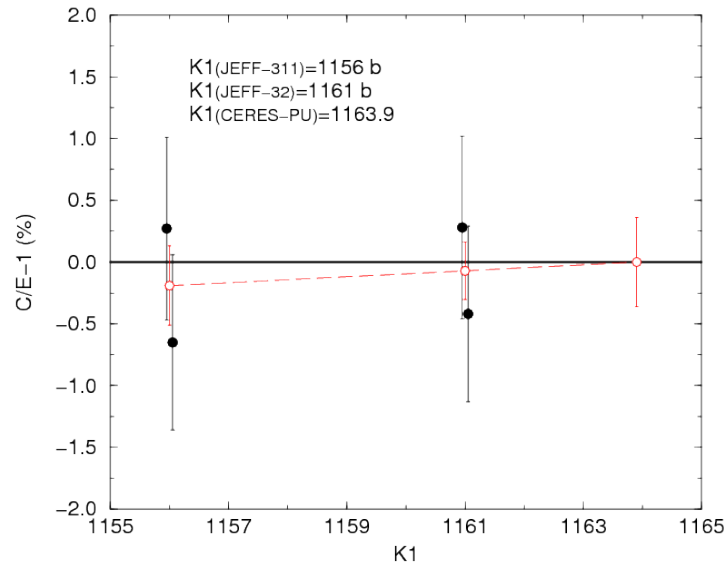
The consistency of the low energy part of the fission and capture cross-sections was investigated with integral data measured in the frame of the CERES-PU programme [37]. The aim of this experimental programme was to measure the reactivity worth  $\delta\rho$  of 12 MOX samples by the oscillation technique in the DIMPLE reactor (AEA, Winfrith). The interpretation was performed with the Monte Carlo code TRIPOLI. Two average values were deduced from the various C/E results. They are reported in Figure 18 as a function of the K1 parameter, already defined in Section 4.3.1. An “experimental” value for the K1 parameter can be deduced from the variation of the reactivity worth obtained by using the <sup>239</sup>Pu evaluation of JEFF-3.1.1 and JEFF-3.2. For small variations of reactivity, we can assume that:

$\Delta(\delta\rho) \propto \Delta(K1)$ , where  $\Delta(\delta\rho)$  and  $\Delta(K1)$  are calculated as follows:

$$\Delta(\delta\rho) = \delta\rho(\text{JEFF-3.1.1}) - \delta\rho(\text{JEFF-3.2}),$$

$$\Delta(K1) = K1(\text{JEFF-3.1.1}) - K1(\text{JEFF-3.2}).$$

**Figure 18: Average (C/E-1) results obtained from the interpretation of the CERES-PU programme carried out in the DIMPLE reactor with the Monte Carlo code TRIPOLI**



Note: The results are expressed as a function of the K1 parameter.

The linear assumption between the variation of reactivity and the variation of K1 leads to an “experimental” value of  $1164 \pm 15$  barns. The latter is in good agreement with the K1 parameter calculated with the resonance parameters established in this work. Results are summarised in Table 7.

**Table 7: Value for the K1 parameter**

Data	K1 parameter
Atlas of Neutron Resonances	1177 barns
JENDL-4	1173 barns
ENDF/B-71	1166 barns
JEFF-3.1	1169 barns
JEFF-3.1.1	1156 barns
WPEC/SG34 (=JEFF-3.2)	1161 barns
This work (CERES-PU)	$1164 \pm 15$ barns

The  $\alpha$  ratio, meaning the ratio of the neutron-induced capture cross-section to the neutron-induced fission cross-section, was investigated in the thermal energy range via Reactivity Temperature Coefficient (RTC) analysis. The analysis was performed with the APOLLO code on the MISTRAL-3 experiment carried out at the EOLE facility of CEA Cadarache. The analysis has shown that the negative bias reported in Table 8 for

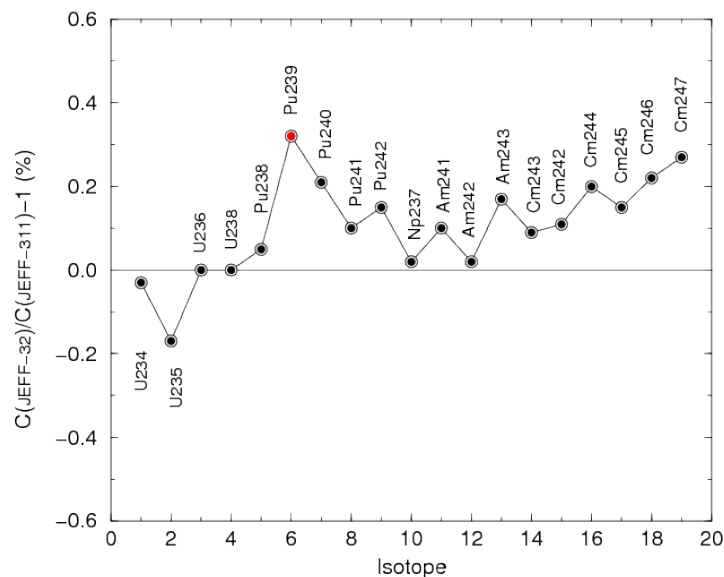
the low-temperature range (below 80°C) is linked to the thermal spectrum shift effect, which could be strongly dependent on the thermal shapes of the capture and fission cross-sections of <sup>239</sup>Pu. New APOLLO calculations with JEFF-3.2 provide a bias on the RTC close to -1.3 pcm/°C, which is an intermediate result between JEFF-3.1 and JEFF-3.1.1. This result indicates that further studies on the energy dependence of the  $\alpha$  ratio in the thermal energy range are needed.

**Table 8: Bias on the reactivity temperature coefficient (pcm/°C) calculated with APOLLO for the MISTRAL-3 programme carried out in the EOLE facility of Cadarache**

Evaluation	10°C-40°C	40°C-80°C	10°C-80°C
JEFF-3.1	-2.3 ± 0.3	-0.8 ± 0.3	-1.6 ± 0.3
JEFF-3.1.1	-0.4 ± 0.5	-1.4 ± 0.5	-1.0 ± 0.4
WPEC/SG34 (=JEFF-3.2)			≈ -1.3

The latest integral validation concerns the impact of the new <sup>239</sup>Pu in fuel inventory calculations in PWR for high burn-up UOX fuels ranging from 65 GWd/t to 85 GWd/t. APOLLO results are reported in Figure 19. A slight increase of about 0.3% of the concentration of <sup>239</sup>Pu is expected. This result confirms that the performances of the new evaluation are equivalent to the <sup>239</sup>Pu evaluation of JEFF-3.1.1.

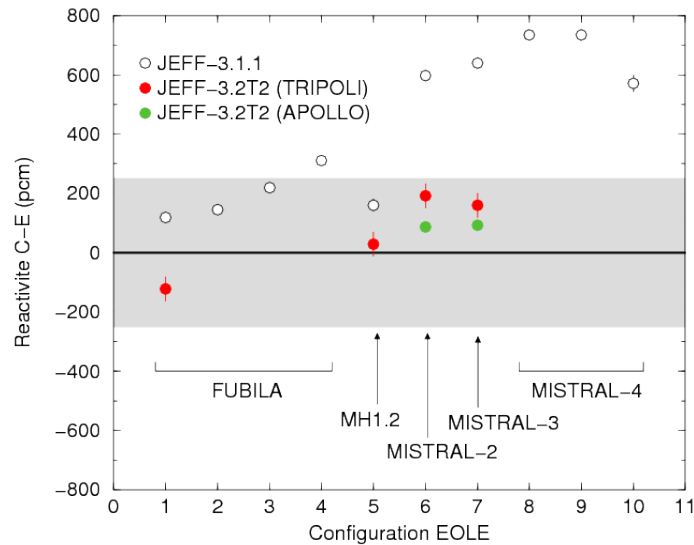
**Figure 19: Fuel inventory calculations in PWR (ALIX-HBU program) for high burn-up between 65 GWd/t and 85 GWd/t**



Note: The calculations were performed with the APOLLO code. JEFF-3.2 contains this new SG34 <sup>239</sup>Pu file.

The evaluation work on <sup>239</sup>Pu was performed not only for criticality studies but also for MOX fuel applications. The new <sup>239</sup>Pu evaluation was tested on various configurations (FUBILA, MH1.2, MISTRAL) measured at the EOLE facility of CEA Cadarache. TRIPOLI and APOLLO results are reported in Figure 20. The C-E results remain below 200 pcm. For the MISTRAL experiments, the significant improvement is linked to <sup>241</sup>Am. The overall agreement demonstrates the quality of the evaluation work performed in collaboration between CEA, ORNL and IRMM on the resolved resonance range of the americium and plutonium isotopes.

**Figure 20: Residual reactivity effect obtained with JEFF-3.1.1 and JEFF-3.2 for various MOX configurations measured in the EOLE facility of CEA Cadarache**



## 6.2 Integral validation based on ENDF/B-VII.1+ SG34 <sup>239</sup>Pu

$K_{\text{eff}}$  C/E calculations have been performed for the described subset of thermal solution benchmarks using ENDF/B-VII.1 (i). For a variety of cross-sections configurations, the <sup>239</sup>Pu data come from (ii) JEFF-3.1.2, (iii) JENDL-4.0 and (iv) SG34 activity (ORNL/CEA <sup>239</sup>Pu file developed for this study). We used ENDF/B-VII.1 cross-sections for all other nuclides in all of these calculations. The results are provided in Table 9.

**Table 9: Calculated  $k_{\text{eff}}$  C/E values**

Benchmark Name	ENDF/B-VII.1 (i)	JEFF-3.1.2 (ii)	JENDL-4.0 (iii)	SG34 (iv)
PST1.4	1.00500(13)	1.00127(6)	1.00588(6)	1.00199(6)
PST4.1	1.00389(11)	0.99907(5)	1.00482(5)	1.00044(5)
PST9	1.01939(5)	1.01367(2)	1.02510(3)	1.01543(2)
PST12.10	1.00402(10)	0.99973(5)	1.00498(3)	1.00083(5)
PST12.13	1.00970(6)	1.00468(3)	1.01069(3)	1.00611(3)
PST18.6	1.00462(11)	1.00153(5)	1.00557(5)	1.00202(5)
PST34.4	1.00254(11)	0.99999(5)	1.00417(5)	0.99922(5)
PST34.15	0.99731(10)	0.99563(5)	0.99844(5)	0.99679(5)
8 assembly average	1.00581	1.00195	1.00746	1.00285

The most direct comparison of these results that demonstrates the improvements from this study is to compare the ENDF/B-VII.1 (i) column and the SG34 (iv) column as only the <sup>239</sup>Pu data differ. The average improvement is nearly 300 pcm, or about 50% of the bias.

The primary differences in the ORNL/CEA file over that in ENDF/B-VII.1 include (i) new resolved resonance parameters, (ii) a revised prompt  $\nu(E)$  below 650 eV and (iii) a revised prompt fission neutron spectrum (PFNS). The latter two differences reflect the use of data from the JEFF-3.1.2 evaluation.



Additional calculations have been performed in which (i) only the revised resolved resonance parameters were inserted into the ENDF/B-VII.1 file, and (ii) both the revised resolved resonance parameters and the revised prompt  $\nu(E)$  up to 650 eV were inserted into the ENDF/B-VII.1 file. With only the RR parameter changed the 8 assembly average is 1.00495; with both RR parameters and prompt  $\nu(E)$  changed the 8 assembly average is 1.00295. These results suggest that of the ~300 pcm shift noted above, about 1/3 of it is attributable to the revised resolved resonance parameters and about 2/3 of it is due to prompt  $\nu(E)$ .

In summary, the <sup>239</sup>Pu data file produced by this Subgroup yields improved  $k_{\text{eff}}$  C/E results compared to those from the ENDF/B-VII.1 and JENDL-4.0 files, but consistent use of ENDF/B-VII.1 data for all other nuclides masks possible improvement for the JEFF community (as seen in Subsection 6.1: *Integral validation based on JEFF-3.1.1 + SG34 <sup>239</sup>Pu*). There are three major changes in this file compared to those found in the ENDF/B-VII.1 file, including (i) revised resolved resonance parameters, (ii) revised prompt  $\nu(E)$  and (iii) revised PFNS. The majority of the observed  $k_{\text{eff}}$  C/E improvement is due to the first two of these changes.

## 7. Investigation on the prompt neutron fission spectrum of the $^{239}\text{Pu}$

The prompt fission neutron spectra (PFNS) are crucial parameters in neutronic calculations. They are very important both for eigenvalue calculations and for radiation shielding calculations because deep penetrating neutrons are born in the fast energy range and any change may have great effects on neutron flux far from the source.

The international evaluation files use the same theoretical model in general but some very different spectra are proposed by other evaluators. The aim of this study is to evaluate the impact of these kinds of spectrum for  $^{239}\text{Pu}$  on some typical benchmarks. The calculations are performed using the Monte Carlo transport code TRIPOLI-4. The considered benchmarks are taken from international databases (ICSBEP, IRPhEP) or MASURCA and EOLE French CEA mock-up experimental facilities.

In the first section, we present graphical comparisons and mathematical characterisations of the different spectra. Then, the TRIPOLI-4  $k_{\text{eff}}$  calculation results with all considered spectra are presented. Finally, an analysis is proposed for some particular thermal cases for which one of the spectra has great effects.

### 7.1 Different $^{239}\text{Pu}$ spectra (PFNS)

A set of different spectra has been studied. The general principle of this study is to use the JEFF-3.1.1 library as a reference, and to replace in the  $^{239}\text{Pu}$  evaluation file the original prompt neutron fission spectra by JENDL-4.0, ENDF/B-VII.0, Maslov and Kornilov spectra [38-40].

As a first consideration, it has to be noted that all international evaluations use a Madland-Nix model to get the final tabulated prompt spectra. They do not use exactly the same parameters (number of chance of fission for example) and some improvements are added (fragments kinetic energy distribution for example). These spectra are very similar. In contrast, Maslov and Kornilov spectra are very different and are based on systematics. All the spectra are presented in Figure 21. They are compared to a Maxwellian distribution with temperature equivalent to 1.3719 MeV.

The spectra are characterised by their mathematical moments:

$$\mu_n = \int E^n \chi(E) dE$$

First moments (mean energy) are shown in Table 10 for different incident neutron energies. The mean energy discrepancy between Kornilov spectrum and JEFF-3.1.1 one is about -2.7% at  $10^{-11}$  MeV and -2.4% at 2 MeV. In Maslov's case, the discrepancy equals -1.0% and -0.8% at these energies, whereas the maximum discrepancies between all international evaluations are 0.2% (at  $10^{-11}$  MeV) and 0.2% (at 2 MeV). In the following sections, only JEFF-3.1.1 spectra will be compared to Maslov and Kornilov ones because all evaluations file spectra (ENDF/B, JEFF, JENDL) give very close results.

**Figure 21: Kornilov spectrum, Maslov spectrum and other international evaluation file spectra compared to a Maxwellian distribution**

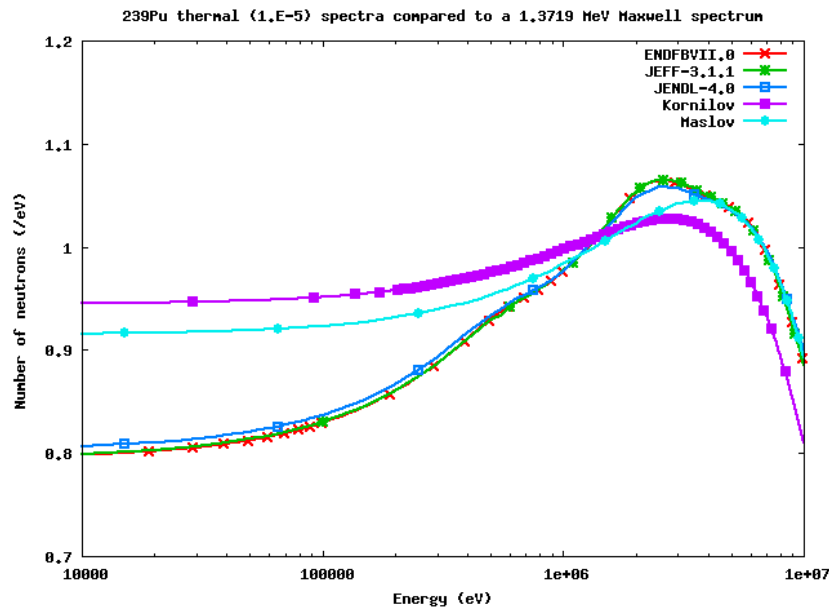


**Table 10: First moment of energy distributions for all spectra**

Energy (MeV)	$10^{-11}$	$10^{-1}$	1	2	5
ENDF/B-VII.0	2.112		2.138	2.163	2.236
JEFF-3.1.1	2.112	2.115	2.140	2.168	2.226
JENDL-4.0	2.116	2.122	2.140	2.165	2.237
Maslov	2.092		2.122	2.152	2.242
Kornilov	2.055		2.084	2.115	2.205

## 7.2 Fast, intermediate and thermal flux experiments

All the presented experiments are characterised by the EALF parameter (Energy of Average Lethargy of Fission).

### 7.2.1 Fast flux spectrum cases

Some fast flux criticality experiments taken in the ICSBEP database have been simulated. They all belong to the PU-MET-FAST class (Plutonium, Metal, Fast spectrum). The results are shown in Table 11. The effect between Maslov or Kornilov spectra and JEFF-3.1.1 spectra has been calculated. EALF is expressed in MeV.

**Table 11: Criticality fast spectrum experiments – Difference between Maslov, Kornilov and JEFF-3.1.1 calculations**

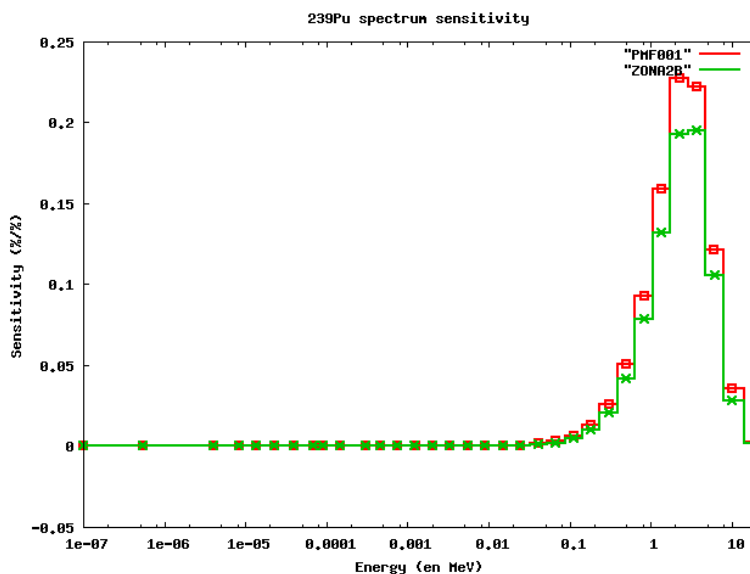
Experiment	EALF (eV)	JEFF-3.1.1 $k_{eff}$	Maslov ( $\Delta$ , pcm)	Kornilov ( $\Delta$ , pcm)
PMF001	1.330	1.00046 (12)	-114 (17)	-279 (17)
PMF002	1.330	1.00433 (5)	-116 (7)	-271 (7)
PMF011	0.108	0.99707 (15)	+41 (21)	-17 (21)
PMF022	1.310	0.99810 (7)	-91 (10)	-227 (10)
PMF024	0.699	0.99982 (8)	-4 (10)	-104 (11)
PMF027	0.090	1.00131 (8)	+10 (11)	+0 (11)
PMF029	1.330	0.99747 (7)	-113 (10)	-264 (10)
PMF031	0.223	1.00333 (8)	-1 (11)	-63 (11)

The fast spectrum mock-up cases are either taken in the IRPhEP database or in the MASURCA experimental programme. The considered IRPhEP experiments are SNEAK7A and SNEAK7B, and the MASURCA results come either from the CIRANO Pu burning cores programme (ZONA 2A, 2B or 2A3 experiments) or from the PRE-RACINE programme dedicated to Super-Phenix reactor (PRE-RACINE I, IIA or IIB experiments). See Table 12.

**Table 12: Mock-up fast spectrum experiments – Difference between Maslov, Kornilov and JEFF-3.1.1 calculations**

Experiment	EALF (eV)	JEFF-3.1.1 $k_{eff}$	Maslov ( $\Delta$ , pcm)	Kornilov ( $\Delta$ , pcm)
ZONA2A	0.192	1.00995 (12)	-149 (17)	-310 (17)
ZONA2B	0.117	1.00918 (3)	-148 (4)	-308 (4)
ZONA2A3	0.142	1.01034 (12)	-140 (17)	-282 (17)
PRE-RAC. I	0.085	1.00446 (12)	-67 (17)	-112 (17)
PRE-RAC. Ila	0.089	1.00431 (12)	-74 (17)	-145 (17)
PRE-RAC. I Ib	0.094	1.00409 (12)	-57 (17)	-157 (17)
SNEAK7A	0.135	1.01001 (2)	-123 (3)	-285 (3)
SNEAK7B	0.141	1.00466 (2)	-181 (3)	-390 (3)

As expected, the effect is important for Kornilov spectra and is negative. Actually, the sensitivity calculations performed with the deterministic system ERANOS/PARIS [41] explain this considerable effect. The sensitivity to high energy (1 MeV and more) is very important and changes in this energy range have a considerable impact on  $k_{eff}$  (see Figure 22).

**Figure 22:  $k_{\text{eff}}$  sensitivities on spectrum for ZONA2B and PU-MET-FAST 001 fast flux spectrum experiments**

### 7.2.2 Intermediate flux spectrum cases

The intermediate flux spectrum experiments PU-COMP-INTER-001 (HISS experiments in Hector reactor), PU-MET-INTER-002 (ZPR-6 assembly 10) and PU-MET-MIXED-001 (or BFS-81 experiment) EALF values cover the energy range from 1 eV to 10 keV. In Table 13, EALF is given in eV.

**Table 13: Criticality intermediate spectrum experiments - Difference between Maslov, Kornilov and JEFF-3.1.1 calculations**

Experiment	EALF (eV)	JEFF-3.1.1 $k_{\text{eff}}$	Maslov ( $\Delta$ , pcm)	Kornilov ( $\Delta$ , pcm)
PCI001	319	1.00860 (11)	-56 (16)	-99 (16)
PMI002	10200	1.03234 (13)	+61 (18)	+85 (18)
PMM001-1	5540	1.00510 (35)	+108 (50)	+200 (49)
PMM001-2	276	1.00470 (20)	+91 (33)	+271 (28)
PMM001-3	61.4	1.00590 (19)	+161 (27)	+332 (29)
PMM001-4	1.34	1.00770 (20)	+98 (29)	+321 (28)
PMM001-5	1.29	1.00719 (19)	106 (26)	+326 (25)

In this test, the effect is positive. For the PCI case, the effect is negative. The experiment corresponds to a  $k_{\infty}$  “measurement” and the leakage effect analysed in the previous section does not occur in this case.

### 7.2.3 Thermal flux spectrum cases

The thermal flux spectrum experiments come either from the ICSBEP database and particularly from the PU-SOL-THERM class (Plutonium, Solution, Thermal spectrum) or from the EOLE French mock-up experimental programme (MISTRAL 100% MOX high moderation core experiments). Results are given in Table 14. The effect of PFNS on PU-SOL-THERM 001, 004, 005, 006 and 007 is very important when using the Kornilov spectrum. This effect is due to large leakage. Some other explanations will be given in the next section. For other cases, the discrepancy is much lower.

**Table 14: Criticality thermal spectrum experiments - Difference between Maslov, Kornilov and JEFF-3.1.1 calculations**

Experiment	EALF (eV)	JEFF-3.1.1 $k_{eff}$	Maslov ( $\Delta$ , pcm)	Kornilov ( $\Delta$ , pcm)
PST001-1	0.089	1.00106 (10)	+411 (14)	+876 (14)
PST001-4	0.154	1.00041 (14)	+394 (20)	+880 (20)
PST001-6	0.367	1.00642 (10)	+366 (14)	+822 (14)
PST004-5	0.054	0.99594 (10)	+328 (14)	+737 (14)
PST005-1	0.055	0.99862 (10)	+318 (14)	+729 (14)
PST005-7	0.068	1.00052 (10)	+318 (14)	+757 (14)
PST006-2	0.053	0.99827 (10)	+294 (14)	+668 (14)
PST007-3	0.272	1.00095 (10)	+373 (14)	+843 (14)
PST007-10	0.107	0.99743 (10)	+388 (14)	+867 (14)
PST012-5	0.043	1.00974 (10)	+54 (12)	+155 (14)
PST012-13	0.043	1.00594 (10)	+50 (14)	+173 (14)

For EOLE mock-up experiments (see Table 15), the impact of the Kornilov and Maslov spectra is less important. Although leakage is quite important in these configurations, the fissile material is different (MOX fuel). The fast neutron fissions effect contributes to the reduction of the discrepancies (see factor  $\epsilon$  in next section).

**Table 15: EOLE mock-up thermal spectrum experiments - Difference between Maslov, Kornilov and JEFF-3.1.1 calculations**

Experiment	JEFF-3.1.1 $k_{eff}$	Maslov ( $\Delta$ , pcm)	Kornilov ( $\Delta$ , pcm)
MISTRAL-2	1.00726 (4)	+37 (6)	+74 (6)
MISTRAL-3	1.00767 (4)	+54 (6)	+110 (6)

### 7.2.4 Physical analysis

An analysis has been performed to understand the considerable effect of Kornilov spectrum in some thermal flux cases. The analysis is based on  $k_{\text{eff}}$  and  $k_{\infty}$  expressions.  $k_{\infty}$  can be written by the well-known Fermi's formula:

$$k_{\infty} = \varepsilon \cdot p \cdot f \cdot \eta$$

where  $\varepsilon$  is the fast energy range amplification factor,  $p$  is the probability to escape to absorption in epithermal energy range,  $f$  is the probability to be absorbed in the fissile zones in the thermal energy range,  $\eta$  is the mean number of fission neutrons per thermal absorption.

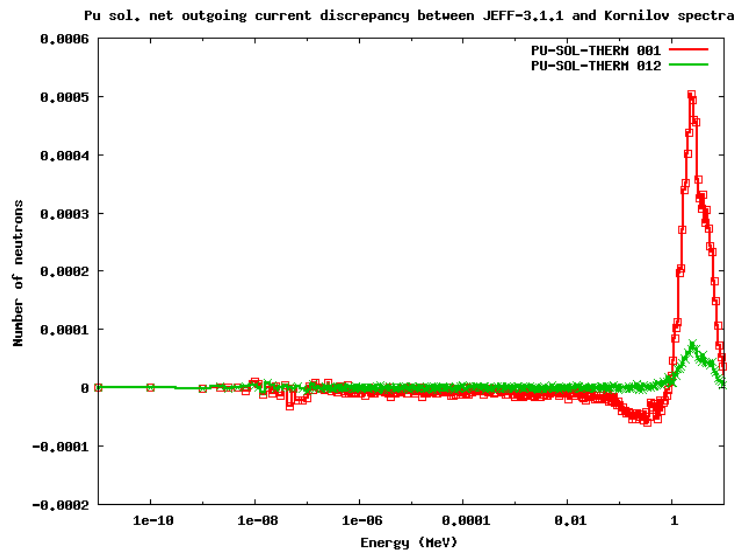
$$k_{\text{eff}} = k_{\infty} / (1 + M^2 B^2),$$

where  $M^2$  is the migration area,  $B^2$  is the buckling. Table 16 shows each of these factors (plus  $\nu$ , the number of neutrons per fission) in the case of JEFF-3.1.1 PFNS and Kornilov PFNS for PU-SOL-THERM-001 case 1.

**Table 16: PU-SOL-THERM-001  $k_{\infty}$  - JEFF-3.1.1 versus Kornilov calculations expressed in PCM**

Factor	JEFF-3.1.1 $k_{\text{eff}}$	Kornilov ( $\Delta$ , pcm)
$\varepsilon$	1.06448 (13)	-14 (13)
$p$	0.89366 (1)	+29 (1)
$f$	0.91994 (12)	0 (11)
$\nu$	2.86787 (34)	-6 (34)
$\eta$	1.92387 (12)	-3 (12)
$k_{\infty}$	1.68364 (32)	+28 (31)

The table shows that all the  $k_{\infty}$  factors (as well as  $k_{\infty}$  itself) are very close. In Figure 23, the fissile zone outgoing net current discrepancy between the two calculation cases is plotted. For the PU-SOL-THERM-001 case, more neutrons leave the fission zone with the JEFF-3.1.1 spectrum and are absorbed in the water reflector. As long as  $B^2$  does not change, the reactivity effect is due to migration area change. This can be explained by the decrease of the <sup>1</sup>H elastic cross-section above 1 MeV. In fact, the decrease of the mean neutron energy with Kornilov spectrum leads to an increase in this averaged cross-section, and consequently a decrease in the migration area.

**Figure 23: Fissile zone outgoing net current discrepancy between JEFF-3.1.1 and Kornilov spectra calculations**

### 7.3 Summary of the PFNS study

This work has shown that the Prompt Fission Neutron Spectra in ENDF/B-VII.0, JEFF-3.1.1 and JENDL-4.0 are very close to each other and that the calculated effective multiplication factors on a set of selected benchmarks are slightly affected by these different evaluations. In contrast, the Maslov and Kornilov spectra may have a considerable effect on some particular configurations. In particular, the calculated impact on the effective multiplication factor can reach +800 pcm in PU-SOL-THERM experiments (with high leakage level) and -300 pcm in fast spectrum experiments for ICSBEP benchmarks and CEA/MASURCA mock-up benchmarks, respectively.



## 8. Conclusions and recommendations

The international effort performed in the framework of this Subgroup enabled delivery of a single set of resonance parameters up to 2.5 keV able to provide good C/E results over a broad set of integral data. The resonance analysis has been performed with the SAMMY code. The thermal capture and fission cross-sections are  $270 \pm 11$  barns and  $747 \pm 7$  barns, respectively. The quoted uncertainties were determined by marginalisation with the CONRAD code. The value of the K1 parameter calculated with the NJOY processing system is 1161 barns.

The large fluctuations of the prompt neutron multiplicities were correctly reproduced with a phenomenological decomposition of the multiplicity that involved the one-step (or direct) fission reaction and the two-step (n, $\gamma$ f) process. Below 2.5 keV, the (n, $\gamma$ f) process was calculated by introducing two additional partial widths ( $\Gamma_{\gamma f} = 7.3$  meV for  $J=0^+$  and  $\Gamma_{\gamma f} = 4.2$  meV for  $J=1^+$ ). The final result was in good agreement with the prompt neutron multiplicity of JEFF-3.1.1.

Performances of the new  $^{239}\text{Pu}$  evaluation were tested over a broad set of integral data (ICSBEP, mock-up experiments performed in the CEA facilities and in power reactors). An overall good agreement was achieved between the calculations and the experimental results. The performances are similar to those of the  $^{239}\text{Pu}$  evaluation of JEFF-3.1.1. More integral feedback will be obtained via the NEA WPEC Subgroups 39 and 40.

The present results allow identifying several priorities for future experimental and evaluation works.

For the resolved resonance range, new transmission measurements of the 1<sup>st</sup> broad s-wave resonance at 0.3 eV are needed as is capture yield over a large energy range. At low energy, the SAMMY/CONRAD analysis relies on a single transmission data set measured by Bollinger in 1958. For the capture cross-section the available data set was measured by Gwin in 1971. High resolution measurements of neutron multiplicity are also required.

Two problems occur during the evaluation work. The first one concerns the Resonance Parameter Covariance Matrix. A concise method for storing and communicating large RPCM is needed. In the present work, an artificial reduced neutron width selection was used to reduce the size of the matrix. The restrictions of the ENDF-6 format are no longer compatible with the possibilities offered by the AGS format developed at the IRMM. The second problem is related to the (n, $\gamma$ f) reaction and the modelling of the fluctuations of prompt neutron multiplicity. The partial widths associated with the (n, $\gamma$ f) reaction have to be included in the evaluated file in order to make possible “on-the-fly” calculations of  $\nu_p(E)$  for a given temperature.

In addition, more work is needed to connect properly the unresolved resonance range with the continuum for the evaluation of cross-sections and model parameters as well as for covariance estimation.

## 9. References

- [1] OECD/NEA, International Handbook of Evaluated Criticality Safety Benchmark Experiments, NEA/NSC/DOC(95)03 (Rev. September 2013).
- [2] F.B. Brown et al., “Advances in the Development and Verification of MCNP5 and MCNP6”, International Conference on Nuclear Criticality, Edinburgh, Scotland, 19-22 September 2011.
- [3] D. Bernard et al., Improvements of the  $^{239}\text{Pu}$  Evaluation for JEFF-3, JEF/DOC-1158, 2006.
- [4] S. van der Marck, Criticality Safety benchmark calculations with MCNP-4C3 using JEFF-3.1 nuclear data, JEFF document JEF/DOC-1107, 2005.
- [5] A. Santamarina et al., The JEFF-3.1.1 Nuclear Data Library - Validation results from JEF-2.2 to JEFF-3.1.1, JEFF Report 22, 2009.
- [6] S.C. van der Marck, “Benchmarking ENDF/B-VII.1, JENDL-4.0 and JEFF-3.1.1 with MCNP6,” Nuclear Data Sheets 113 (2012) 2935.
- [7] N.M. Larson, ORNL0TM-91790R7, Oak Ridge National Laboratory, 2006.
- [8] R.E. MacFarlane and D.W. Muir, Los Alamos National Laboratory; <http://t2.lanl.gov/nis/codes/njoy99>.
- [9] M. Coste-Delclaux et al., “GALILÉE: A nuclear data processing system for transport, depletion and shielding codes”, WONDER 2009 (Workshop On Nuclear Data Evaluation for Reactor applications), Cadarache, France, 2009.
- [10] F. Malvagi et al., Overview of TRIPOLI4 Version 7 Continuous-energy Monte Carlo Transport Code, Proceedings of ICMPP 2011 (2011).
- [11] R. Sanchez et al., “Apollo2 year 2010”, Nuclear Engineering and Technology, Vol.42 No.5 October 2010.
- [12] H. Derrien, G. De Saussure, and R.B. Perez, “R Matrix Analysis of  $^{239}\text{Pu}$  Neutron Cross Sections in the Energy Range up to 1000 eV”, Nucl. Sci. Eng. 106 (1990) 434.
- [13] H. Derrien, “R-Matrix Analysis of  $^{239}\text{Pu}$  Neutron Transmission and Fission Cross Sections in Energy Range from 1.0 keV to 2.5 keV”, J. Nucl. Sci. Technol. 30 (1993) 845.
- [14] J.A. Harvey et al., Proc. Int. Conf. Nuclear Data for Science and Technology, Mito, Japan May 30-June 3, 1988.
- [15] H. Derrien, L.C. Leal, and N.M. Larson, “Neutron Resonance Parameters and Covariance Matrix of  $^{239}\text{Pu}$ ,” ORNL/TM-2008/123, September 2008.
- [16] D. Bernard et al., “ $^{239}\text{Pu}$  Nuclear Data Improvements in Thermal and Epithermal Neutron Ranges,” International Conference on Nuclear Data for Science and Technology, Nice, France April-22-27, 2007.
- [17] L.C. Leal et al. “R-Matrix Analysis of  $^{235}\text{U}$  Neutron Transmission and Cross Section in the Energy 0 to 2.25 keV,” Nucl. Sci. Eng. 131. 230 (February 1999).
- [18] L. Erradi, A. Santamarina, and O. Litaize, “The Reactivity Temperature Coefficient Analysis in Light Water Moderated UO<sub>2</sub> and UO<sub>2</sub>-PuO<sub>2</sub> Lattices”, Nucl. Sci. Eng. 144, 47-74 (2003).
- [19] L.M. Bolinger, R.E. Cote, and G.E. Thomas, Bul. Am. Phys. Soc. 1, 187 (K5) 1956.
- [20] C. Wagemans et al., Proc. Int. Conf. Nuclear Data for Science and Technology, Mito, Japan May 30-June 3, 1988.

- [21] R. Gwin et al., “Simultaneous Measurement of the Neutron Fission and Absorption Cross Sections of Plutonium-239 Over the Energy Region 0.02 eV to 30 keV”, Nucl. Sci. Eng. 45, 25 (1971).
- [22] S.F. Mughabghab, “Atlas of Neutron Resonance Parameters and Thermal Cross Sections, Z=1-100,” Elsevier 2006.
- [23] SCALE: A Modular Code System for Performing Standardized Computer Analyses for Licensing Evaluations, NUREG/CR-0200, Rev. 7 (ORNL/NUREG/CSD-2/R7), Vols I, II, and III (May 2004).
- [24] C. De Saint Jean et al., “Uncertainty Evaluation of Nuclear Reaction Model Parameters Using Integral and Microscopic Measurements with the CONRAD Code”, Journal of the Korean Physical Society, 59 (2011) 1276-1279.
- [25] C. De Saint Jean et al., “A Monte Carlo Approach to Nuclear Model Parameter Uncertainties Propagation”, Nucl. Sci. Eng. 161, 363 (2009).
- [26] B. Habert et al., “Retroactive Generation of Covariance Matrix of Nuclear Model Parameters Using Marginalization Techniques”, Nucl. Sci. Eng. 166, 276 (2010).
- [27] G. Noguere et al., “Zero Variance Penalty Model for the Generation of Covariance Matrices in Integral Data Assimilation Problems”, Nucl. Sci. Eng. 172, 164 (2012).
- [28] E. Lynn et al., “On the slow neutron, gamma-fission reaction”, Phys. Lett. 18, 31 (1965).
- [29] S. Bjørnholm and E. Lynn, “The double-humped fission barrier”, Rev. Mod. Phys. 52, 725 (1980).
- [30] G. LeCoq, Evaluation des données neutroniques pour le  $^{239}\text{Pu}$ , PhD thesis, Orsay, France, 1967.
- [31] H. Derrien, Etudes des sections efficaces de réaction des neutrons de résonance avec  $^{239}\text{Pu}$ , PhD Thesis, Orsay, France, 1973.
- [32] D. Shackleton, Etude des neutrons et des rayons gamma émis lors de la fission induites dans  $^{235}\text{U}$  et  $^{239}\text{Pu}$  par neutrons lents: mise en évidence de la réaction (n, $\gamma$ f), Orsay, France, 1974.
- [33] J.E. Lynn, Systematics for neutron reactions of the actinide nuclei, AERE-R7468 (1974).
- [34] O. Bouland et al., “R-matrix analysis and prediction of low-energy neutron-induced fission cross sections for a range of Pu isotopes”, Phys. Rev. C 88, 054612 (2013).
- [35] E. Fort et al., “Evaluation of nu-p for  $^{239}\text{Pu}$ : Impact for Applications of the Fluctuations at Low Energy”, Nucl. Sci. Eng. 99, 375 (1988).
- [36] R. Gwin et al., “Measurements of the Energy Dependence of Prompt Neutron Emission from  $^{233}\text{U}$ ,  $^{235}\text{U}$ ,  $^{239}\text{Pu}$ , and  $^{241}\text{Pu}$  for  $E_n = 0.005$  to 10 eV Relative to Emission from Spontaneous Fission of  $^{252}\text{Cf}$ ”, Nucl. Sci. Eng. 87, 381 (1984).
- [37] P. Leconte et al., submitted to PHYSOR 2014.
- [38] K Shibata et al., JENDL-4.0: A New Library for Nuclear Science and Engineering, Journal of Nuclear Science and Technology 48(1), page 1-30 (2011).
- [39] M.B. Chadwick et al., ENDF/B-VII.0: Next Generation Evaluated Nuclear Data Library for Nuclear Science and Technology, Nuclear Data Sheets 107, page 2931–3060 (2006).
- [40] R. Capote et al., Summary report, consultants’ meeting on Prompt Fission Neutron Spectra of major actinides, IAEA INDC(NDS)-0541 (2008).
- [41] R. Letellier, C. Suteau, D. Fournier, J-M. Ruggieri, High Order Discrete Ordinate Transport in Hexagonal Geometry: a New Capability in ERANOS, Il Nuovo Cimento, 33C, (2010).